AIMS Mathematics, 11(4): 11437–11472.
DOI: 10.3934/math.2026471
Received: 03 March 2026
Revised: 04 April 2026
Accepted: 14 April 2026
Published: 24 April 2026

https://www.aimspress.com/journal/Math

Research article

The generalized discrete Burr–Hatke exponential distribution: Mathematical characterization, reliability analysis, and applications to censored actuarial, clinical, and agricultural data

Mohamed S. Eliwa[1,2], **Hend S. Shahen**[3,*] **and Mahmoud El-Morshedy**[3]

[1] Department of Statistics and Operations Research, College of Science, Qassim University, Saudi Arabia; m.eliwa@qu.edu.sa
[2] Department of Mathematics, Faculty of Science, Mansoura University, Mansoura 35516, Egypt
[3] Department of Mathematics, College of Science and Humanities in Al-Kharj, Prince Sattam Bin Abdulaziz University, Al-Kharj 11942, Saudi Arabia

* **Correspondence:** Email: h.shahen@psau.edu.sa.

Abstract: This paper introduces a novel and highly flexible two-parameter discrete distribution designed for modeling complex count data. We comprehensively derive its statistical, reliability, and actuarial properties, establishing key metrics including moments, entropy, stochastic orders, and risk measures such as value-at-risk and tail-value-at-risk. The proposed model is particularly adept at capturing right-skewed, overdispersion data characterized by outliers and varying kurtosis. Notably, its hazard rate function accommodates diverse shapes, including increasing, decreasing, unimodal, bathtub, and J-shaped, while asymptotically approaching a constant to exhibit geometric-like memoryless properties. Model parameters are estimated via the maximum likelihood method for both complete and censored datasets. Additionally, we develop computationally efficient Monte Carlo simulation strategies leveraging these versatile hazard profiles. Empirical applications across actuarial science, clinical nephrology, and agricultural entomology demonstrate the model's superior efficacy in capturing extreme values when compared to existing competing distributions.

Keywords: statistical model; failure analysis; reliability aging classes; actuarial risk measures; Monte Carlo simulation; censored data; data analysis
Mathematics Subject Classification: 62E99, 62E15

1. Introduction

Modelling lifetime data is crucial in reliability engineering, survival analysis, and actuarial research. Although continuous probability distributions have historically prevailed in many domains,

discrete models are becoming increasingly essential. Data is sometimes inherently discrete or categorized into discrete intervals due to measurement limitations; thus, employing continuous models on such data may result in skewed risk evaluations and erroneous conclusions. Moreover, traditional discrete distributions frequently lack the adaptability necessary to effectively depict intricate behaviors such as overdispersion, heavy tails, or nonmonotonic hazard rates. To address these constraints, contemporary statistical research primarily emphasises the creation of highly adaptable discrete distributions through the discretization of existing continuous models or the alteration of conventional discrete frameworks. For instance, the discrete Rayleigh distribution was initially introduced by [1], establishing a foundation for the analysis of discrete reliability data. Subsequently, researchers in [2] developed the discrete gamma distribution and demonstrated its utility across several scenarios. In 2014, the researchers in [3] enhanced the modified Weibull distribution for failure data modeling by adapting it to a discrete framework. The researchers in [4] further developed the field by introducing the exponentiated discrete Weibull distribution and demonstrating its practical applications.

Recent, research by [5] examined the discrete Bilal distribution, focusing on its characteristics and applicability in integer-valued autoregressive contexts. In their extensive examination of discrete distributions, researchers in [6] integrated current advancements and emphasized the numerous applications of these distributions. The researchers in [7] proposed new discrete trigonometric distributions for count data analysis, so augmenting the repertoire of discrete modeling techniques. The researchers in [8] introduced a discrete extension of the exponential type II distribution, highlighting its applicability in dependability theory. Collectively, these studies exhibit ongoing efforts to enhance the precision of models employed with specialized data structures, particularly those pertaining to biological or ecological contexts. These recent improvements demonstrate that discrete distribution theory remains pertinent and beneficial for addressing contemporary data challenges across several domains, while also expanding the analytical repertoire available to analysts. In accordance with ongoing endeavours to enhance distribution theory, the Burr–Hatke differential equation has recently surfaced as a significant instrument for producing adaptable probability models. The researchers in [9] introduced the discrete Burr–Hatke exponential (DBuE) distribution for the explicit purpose of representing count data. Nonetheless, as a univariate model, the DBuE frequently demonstrates inadequacy for applications necessitating stringent tail modeling, such as actuarial risk management, or for accurately representing intricate aging dynamics in reliability studies. This research presents a unique flexible discrete probability model developed by employing the exponentiated methodology within the DBuE framework to address this gap. The cumulative distribution function (CDF) of the baseline DBuE distribution is articulated as

$$K(x;\theta) = 1 - \frac{\theta^{x+1}}{1-(x+1)\ln\theta}; \qquad 0 < \theta < 1,\ x = 0, 1, 2, 3 \ldots, \tag{1.1}$$

where θ is a shape parameter. To generalize this baseline model and incorporate the additional parameter necessary for capturing intricate data structures, we utilize the exponentiated-G family. Within this context, an exponentiated distribution is characterized by the following equation:

$$F(x;\alpha,.) = [K(x;.)]^{\alpha}; \qquad \alpha > 0, \tag{1.2}$$

where $K(x;.)$ represents the CDF of the random variable X. This exponentiation approach enhances the adaptability of the baseline distribution, facilitating superior modeling of outliers, skewness, and

intricate tail and hazard rate characteristics. The supplementary shape parameter α enhances control over the distributional form, allowing it to encompass a broader spectrum of data features. When $\alpha > 1$, the distribution is increasingly more concentrated and skewed toward elevated values. When $0 < \alpha < 1$, it expands the distribution toward lower values to more effectively capture underdispersion or bounded patterns. This technology has been widely utilized to broaden numerous classical discrete distributions. Notable instances in the discrete domain encompass the exponentiated geometric distribution for overdispersion count data [10], the exponentiated Poisson for queuing and risk assessment [11], and the exponentiated negative binomial for epidemiological and rare-event data [12]. Additional significant contributions encompass the exponentiated discrete Weibull distribution [4], the exponentiated discrete Lindley distribution [13], and the references cited therein.

A novel discrete generalization to the DBuE distribution is presented, motivated by the flexibility and effectiveness of the exponentiation method demonstrated in these studies. Thus, a new extension known as the exponentiated DBuE (EDBuE) distribution is presented using Eqs (1.1) and (1.2). The CDF of the proposed model can be expressed as:

$$F(x;\alpha,\theta) = \left(1 - \frac{\theta^{x+1}}{1-(x+1)\ln\theta}\right)^{\alpha};\ x \in \mathbb{N}_0, \tag{1.3}$$

where $\alpha > 0,\ 0 < \theta < 1$ and $\mathbb{N}_0 = 0, 1, 2, 3, ...$ The corresponding probability mass function (PMF) of Eq (1.3) can be proposed as

$$f(x;\alpha,\theta) = \left(1 - \frac{\theta^{x+1}}{1-(x+1)\ln\theta}\right)^{\alpha} - \left(1 - \frac{\theta^{x}}{1-x\ln\theta}\right)^{\alpha};\ x \in \mathbb{N}_0. \tag{1.4}$$

The rationale for implementing the suggested discrete probability model is based on its theoretical manageability and practical adaptability. First, the distribution has closed-form expressions for its PMF, CDF, survival function, and hazard rate function. In distribution theory, it is very useful to have explicit analytical forms because they make theoretical derivations easier, make statistical inference easier, and make it easier to use in real-world situations. Because of these easy-to-use features, the model can be used in many fields, such as engineering, reliability analysis, actuarial science, risk assessment, and medical statistics. A second important reason is that its hazard rate function is very flexible. The hazard rate can take on different shapes, such as increasing, decreasing, unimodal, J-shaped, and bathtub-shaped, depending on how the parameters are set up. This kind of flexibility is especially useful in studies of reliability and survival, where real-world failure mechanisms often show different and complicated behaviors over time. The suggested model can thus depict a wide range of lifetime and failure attributes observed in practice. Another interesting thing about the distribution is that it can show heavy-tailed behavior for some values of the parameters. This characteristic renders the model particularly appropriate for count data that includes extreme observations, outliers, or abnormally high frequencies. In numerous practical scenarios, empirical data diverge from the premises of classical thin-tailed discrete models. In these instances, a distribution characterized by heavier tails can enhance robustness and offer a more accurate depiction of the underlying stochastic framework. In addition, the proposed model demonstrates appealing properties under several entropy measures, including Shannon entropy, Rényi entropy, and related information-based criteria. Different parameter settings create different uncertainty structures, which gives us more information about the model's variability and randomness. This adaptability based on

entropy makes the model more useful in situations where measuring uncertainty is very important. Also, the distribution's structure lets it handle many different types of data patterns, such as modal behavior, strong peaks, unusual frequencies, skewness, and overdispersion. Its adaptability allows it to represent both light-tailed and heavy-tailed environments, rendering it appropriate for data with varied kurtosis traits and asymmetric counting patterns. In general, the suggested discrete distribution is a good addition to the current set of discrete models. It is a competitive and useful alternative to many existing distributions in the literature because it is mathematically easy to work with, has flexible hazard behavior, can handle heavy tails, and can be used in many different situations.

Building upon this theoretical versatility, it is crucial to establish robust inference procedures that accommodate common data limitations found in these practical applications. Consequently, this paper provides a significant contribution by the meticulous analysis of parameter estimation under type II censoring, in addition to its theoretical and structural merits. This sampling method is commonly utilized in reliability analysis and survival studies, where experimentation concludes upon the observation of a specified number of failures. Consequently, only the least ordered observations are recorded, and the remaining units are categorized as suppressed. This method is particularly beneficial in life-testing investigations, as it significantly reduces both time and cost while preserving sufficient information for reliable statistical inference. type II censoring is widely utilized in industrial reliability testing, clinical research, and engineering scenarios when comprehensive data collecting is either unfeasible or prohibitively costly. For additional details, refer to [14–18], and the references cited therein.

The following sections are organized as outlined below: Section 2 delineates the mathematical characteristics and configurations of the EDBuE distribution. Section 3 evaluates the failure and reversed failure rate functions, and Section 4 investigates aging and reliability features. Section 5 provides a study of essential actuarial indicators. Section 6 elucidates further statistical features, encompassing moments and entropy metrics. Section 7 addresses maximum likelihood estimates for both complete and censored data, with performance assessment conducted by Monte Carlo simulations in Section 8. Section 9 applies the model to empirical datasets to illustrate its adaptability, and Section 10 offers concluding observations.

2. Shape analysis: Asymptotics, convexity, and visualization

To simplify the notation, because $\ln\theta < 0$, we substitute $\lambda = -\ln\theta$. Consequently, the auxiliary function $u(x)$ can be expressed as

$$u(x) = \frac{\theta^x}{1 - x\ln\theta} = \frac{e^{-\lambda x}}{1 + \lambda x}. \tag{2.1}$$

The CDF associated with this PMF can be viewed as $F(x) = (1 - u(x+1))^\alpha$. Specifically, Eq (1.4) is of the form $f(x) = G(x+1) - G(x)$ where $G(x) = (1 - u(x))^\alpha$.

2.1. Asymptotic behavior ($x \to \infty$)

We analyze the behavior of the PMF $f(x;\alpha,\theta)$ as $x \to \infty$. Because $\lambda > 0$, as $x \to \infty$, $u(x) \to 0$. We employ the binomial approximation $(1-y)^\alpha \approx 1 - \alpha y$ for small y

$$G(x) = (1 - u(x))^\alpha \approx 1 - \alpha u(x). \tag{2.2}$$

Substituting this into the expression for PMF

$$\begin{aligned} f(x;\alpha,\theta) &= G(x+1) - G(x) \\ &\approx (1-\alpha u(x+1)) - (1-\alpha u(x)) \\ &= \alpha\,(u(x) - u(x+1))\,. \end{aligned} \tag{2.3}$$

Now we analyze the difference $u(x) - u(x+1)$

$$u(x) - u(x+1) = \frac{\theta^x}{1+\lambda x} - \frac{\theta^{x+1}}{1+\lambda(x+1)}. \tag{2.4}$$

For large x, $1 + \lambda x \approx \lambda x$. Thus,

$$\begin{aligned} u(x) - u(x+1) &\approx \frac{\theta^x}{\lambda x} - \frac{\theta^{x+1}}{\lambda x} \\ &= \frac{\theta^x}{\lambda x}(1-\theta). \end{aligned} \tag{2.5}$$

Therefore, the asymptotic approximation of the PMF is

$$f(x;\alpha,\theta) \sim \frac{\alpha(1-\theta)}{\lambda} \cdot \frac{\theta^x}{x} \quad \text{as } x \to \infty. \tag{2.6}$$

This confirms that the tail of the distribution decays geometrically (exponentially) with a polynomial correction factor of order $O(x^{-1})$.

2.2. Convexity property

A discrete function $f(x)$ is strictly convex if its second-order forward difference is positive

$$\Delta^2 f(x;.) = f(x+2;.) - 2f(x+1;.) + f(x;.) > 0. \tag{2.7}$$

To determine the convexity, we examine the extension of the asymptotic form derived above. Let $y(t) = Ct^{-1}\theta^t$ for $t > 0$ and constant $C > 0$. The second derivative with respect to t is

$$y''(t) = C\theta^t \left[\frac{(\ln\theta)^2}{t} - \frac{2\ln\theta}{t^2} + \frac{2}{t^3} \right]. \tag{2.8}$$

Substituting $\ln\theta = -\lambda$:

$$y''(t) = C\theta^t \left[\frac{\lambda^2}{t} + \frac{2\lambda}{t^2} + \frac{2}{t^3} \right]. \tag{2.9}$$

Given that $\alpha > 0$, $\theta \in (0,1)$, and $t > 0$, it follows that $\lambda > 0$. Therefore, all elements within the brackets are positive. Consequently, $y''(t) > 0$ for any $t > 0$. The analysis indicates that the PMF is asymptotically convex due to the predominance of the θ^x term for $x \to \infty$. Although this convexity is an asymptotic characteristic for general α, for $0 < \alpha \leq 1$, the function is absolutely convex and monotonically decreasing across the whole support $x \in \mathbb{N}_0$. If $\alpha > 1$, the function may initially exhibit unimodality, but it ensures convexity in the tail as $x \to \infty$. Figure 1 depicts the PMF for various parameter configurations for α and θ. The graphic illustrates the versatile characteristics of

the distribution, encompassing severely right-skewed, moderately dispersed, and almost symmetric patterns throughout the support.

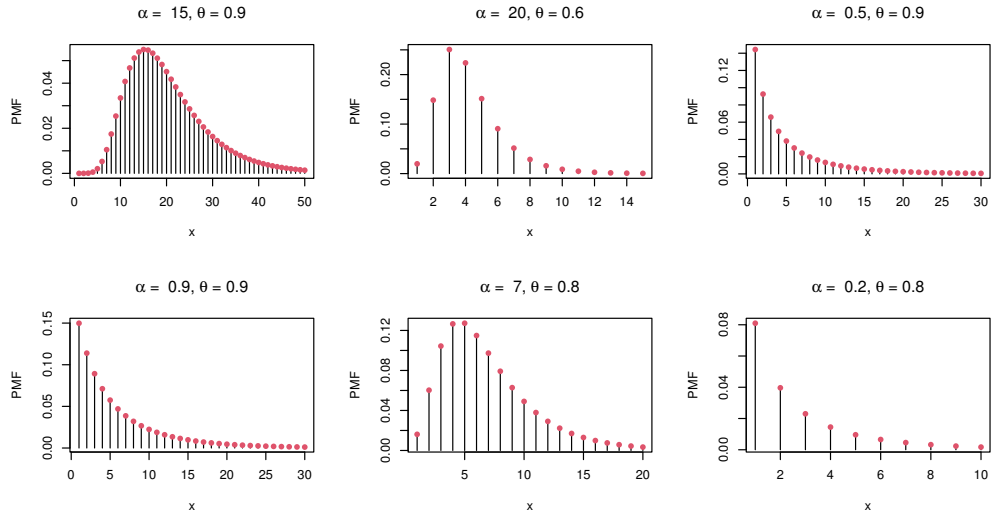

Figure 1. Various shapes for the PMF of the EDBuE distribution.

3. Asymptotic behavior and convexity of the failure rate and reversed failure rate functions

The hazard rate function (HRF) of the EDBuE model can be expressed as

$$h(x;\alpha,\theta) = \frac{(1-u(x+1))^{\alpha} - (1-u(x))^{\alpha}}{1-(1-u(x))^{\alpha}};\ x = 0,1,2,3\ldots. \tag{3.1}$$

To analyze the asymptotic behavior as $x \to \infty$, we employ the binomial expansion $(1-y)^{\alpha} \approx 1-\alpha y$ for tiny y (given that $u(x) \to 0$): The numerator approximates to $\alpha\,[u(x)-u(x+1)]$, and the denominator approximates to $1-(1-\alpha u(x)) = \alpha u(x)$. Substituting these estimates into $h(x;\alpha,\theta)$

$$\begin{aligned}\lim_{x\to\infty} h(x;\alpha,\theta) &= \lim_{x\to\infty} \frac{\alpha\,[u(x)-u(x+1)]}{\alpha u(x)} \\ &= \lim_{x\to\infty}\left(1-\frac{u(x+1)}{u(x)}\right).\end{aligned} \tag{3.2}$$

Analyzing the ratio of successive auxiliary terms

$$\frac{u(x+1)}{u(x)} = \frac{\theta^{x+1}}{1+\lambda(x+1)}\cdot\frac{1+\lambda x}{\theta^{x}} = \theta\left(\frac{1+\lambda x}{1+\lambda x+\lambda}\right). \tag{3.3}$$

As $x \to \infty$, the fraction approaches 1. Therefore

$$\lim_{x\to\infty} h(x;\alpha,\theta) = 1-\theta. \tag{3.4}$$

The HRF asymptotically approaches a constant value of $1-\theta$. This indicates that for high x, the distribution demonstrates memoryless characteristics akin to the geometric distribution. The

memoryless property is important for both statistical modelling and real-world uses. In reliability analysis, it is especially pertinent for components functioning within their designated lifespan, characterized by a constant failure rate following the initial burn-in phase. In queueing theory, the memoryless structure makes it easier to analyze and understand service mechanisms and system performance. It is also useful for modelling count data, especially for processes where events happen at random times with the same chance. These features make the proposed model more useful in a number of fields. To ascertain the convexity and form, examine the asymptotic approximation $h(x) \approx 1 - \theta\rho(x)$, where $\rho(x) = \frac{1+\lambda x}{1+\lambda x+\lambda}$. Calculating the derivative of $\rho(x)$ with respect to x

$$\rho'(x) = \frac{\lambda(1 + \lambda x + \lambda) - \lambda(1 + \lambda x)}{(1 + \lambda x + \lambda)^2} = \frac{\lambda^2}{(1 + \lambda x + \lambda)^2} > 0. \tag{3.5}$$

Because $\rho(x)$ is increasing, $h(x)$ is decreasing in the tail. Examining the second derivative of the approximation

$$\frac{d^2}{dx^2}h(x) \approx -\theta\rho''(x) = -\theta\left[-2\frac{\lambda^3}{(1 + \lambda x + \lambda)^3}\right] > 0. \tag{3.6}$$

The HRF is asymptotically strictly convex and monotonically decreasing, converging to the constant $1 - \theta$ from above. Figure 2 depicts the hazard rate graphs for various combinations of α and θ. The parameter α regulates the dynamics of form and monotonicity, whereas θ dictates the asymptotic behavior. These graphs illustrate the model's versatility by exhibiting increasing, decreasing, bathtub, and unimodal patterns, thus affirming its adaptability to diverse lifetime data trends.

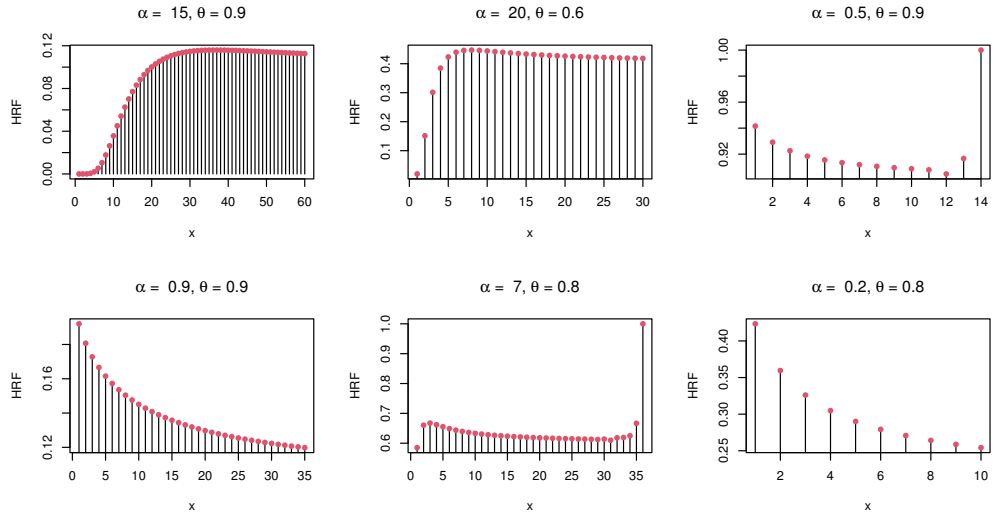

Figure 2. Various shapes for the HRF of the EDBuE distribution.

For the reversed hazard rate function (RHRF), it can be formulated as

$$r(x; \alpha, \theta) = 1 - \frac{(1 - u(x))^\alpha}{(1 - u(x + 1))^\alpha}. \tag{3.7}$$

As $x \to \infty$, the CDF $F(x; \alpha, \theta) \to 1$. Consequently, the behavior of $r(x; \alpha, \theta)$ is dominated by the PMF

of the proposed model where

$$\lim_{x\to\infty} r(x;\alpha,\theta) = \frac{\lim f(x;\alpha,\theta)}{1} = 0. \tag{3.8}$$

Using the asymptotic derived for the PMF

$$r(x;\alpha,\theta) \sim f(x;\alpha,\theta) \sim \frac{\alpha(1-\theta)}{\lambda}\frac{\theta^x}{x}. \tag{3.9}$$

Subsequently, the RHRF diminishes to zero in a geometric manner. Given that $r(x;\alpha,\theta) \approx f(x;\alpha,\theta)$ for large x, and that we have previously demonstrated the asymptotic convexity of $f(x;\alpha,\theta)$ (governed by the factor θ^x), it follows that

$$\Delta^2 r(x;\alpha,\theta) > 0 \quad \text{for sufficiently large } x. \tag{3.10}$$

Consequently, the RHRF exhibits asymptotic convexity and is monotonically declining.

4. Aging properties and reliability class: Theory and methods

In reliability theory, categorizing distributions according to their aging characteristics is essential for comprehending the longevity of systems. This study examines the stochastic ordering of the EDBuE distribution for the shape parameter α and correlates these results with recognized reliability classes. In the context of stochastic ordering, let $X_1 \sim \text{EDBuE}(\alpha_1,\theta)$ and $X_2 \sim \text{EDBuE}(\alpha_2,\theta)$ represent two random variables. We reiterate the definitions of the partial orderings:

- Likelihood ratio order ($X_1 \leq_{lr} X_2$): Holds if $f(x;\alpha_2,\theta)/f(x;\alpha_1,\theta)$ is not decreasing in x.
- Hazard rate order ($X_1 \leq_{hr} X_2$): Holds if $h(x;\alpha_1,\theta) \geq h(x;\alpha_2,\theta)$ for all x.
- Stochastic order ($X_1 \leq_{st} X_2$): Holds if $S(x;\alpha_1,\theta) \leq S(x;\alpha_2,\theta)$ for all x, where $S(\cdot)$ is the survival function.

The hierarchy of these orders is known as

$$X_1 \leq_{lr} X_2 \implies X_1 \leq_{hr} X_2 \implies X_1 \leq_{st} X_2. \tag{4.1}$$

Proposition 4.1. *Let X_1 and X_2 adhere to the EDBuE distribution characterized by parameters (α_1,θ) and (α_2,θ), respectively. If $\alpha_1 > \alpha_2$, then X_1 is less than or equal to X_2 in the stochastic order.*

Proof. Let the survival function (SF) of the EDBuE distribution be approximated or represented in the form $S(x;\alpha) \approx [1-u(x)]^\alpha$, where $u(x) \in (0,1)$ is the base probability term defined previously. Consider the ratio of the survival functions for $\alpha_1 > \alpha_2$:

$$\frac{S(x;\alpha_1)}{S(x;\alpha_2)} = \frac{[1-u(x)]^{\alpha_1}}{[1-u(x)]^{\alpha_2}} = [1-u(x)]^{\alpha_1-\alpha_2}. \tag{4.2}$$

Because $0 < 1-u(x) < 1$ and $\alpha_1 - \alpha_2 > 0$, it follows that $[1-u(x)]^{\alpha_1-\alpha_2} < 1$. Thus, $S(x;\alpha_1) < S(x;\alpha_2)$ for all x, which implies $P(X_1 > x) \leq P(X_2 > x)$. Therefore, X_1 is stochastically smaller than X_2 ($X_1 \leq_{st} X_2$). □

As the parameter α escalates, the likelihood of the system enduring beyond time x diminishes. A smaller α signifies a heavier tail or a more enduring system. The geometric convexity and asymptotic behavior established in the preceding sections enable the classification of the EDBuE distribution into common reliability categories: increasing failure rate (IFR) and decreasing failure rate (DFR).

Definition 4.2. *A discrete distribution is said to belong to the DFR class if its PMF $f(x;.)$ is log-convex, that is, $f(x+1;.)^2 \leq f(x;.)f(x+2;.)$ for all x, or equivalently, if the HRF $h(x;.)$ is nonincreasing.*

Definition 4.3. *A distribution belongs to the IFR class if $f(x;.)$ is log-concave, that is, $f(x+1;.)^2 \geq f(x;.)f(x+2;.)$, implying $h(x;.)$ is nondecreasing.*

Through the convexity analysis of $\Delta^2 f(x;.)$, numerous significant characteristics of the EDBuE distribution may be determined. Concerning the asymptotic DFR property, it has been demonstrated that as $x \to \infty$, $f(x) \sim C\frac{\theta^x}{x}$. The tail behavior is log-convex because θ^x is log-linear, and the term $1/x$ contributes convexity, so we establish that the EDBuE distribution is asymptotically DFR. This conclusion corresponds with the result that $\lim_{x\to\infty} h(x) = 1-\theta$ stays invariant, signifying the threshold of the DFR class. Moreover, the overall behavior of the distribution is contingent upon its parameters. For $0 < \alpha \leq 1$, the PMF exhibits global convexity and monotonic decrease, signifying that the EDBuE distribution is classified inside the DFR category for this parameter interval. When $\alpha > 1$, the HRF displays bathtub or unimodal (inverted bathtub) characteristics, transitioning from IFR behavior during initial failures to DFR behavior in the wear-out or steady-state phase. In summary, the EDBuE distribution proficiently connects the reliability classes. It is not confined to a singular class, whether strictly IFR or DFR, but instead offers a versatile framework that finally converges into the DFR class as $x \to \infty$, irrespective of the initial parameter α.

5. Actuarial measures: Mathematical and numerical analysis

In actuarial science and risk management, it is crucial to characterize the tail behavior of a loss distribution. We analyze two essential characteristics of the EDBuE distribution: value-at-risk (VaR) and tail-value-at-risk (TVaR). These measures assess the potential risk of a system or portfolio. For further details, refer to [19].

5.1. Value-at-risk

The VaR at a confidence level $q \in (0,1)$ denotes the limit beyond which the probability of incurring a loss surpasses $1-q$. For the discrete EDBuE distribution, VaR_q is defined as the minimal integer x that fulfills the cumulative distribution criterion

$$\text{VaR}_q = \inf\{x \in \mathbb{N}_0 : F(x;\alpha,\theta) \geq q\}. \tag{5.1}$$

Substituting the CDF of the EDBuE distribution

$$\left(1 - \frac{\theta^{x+1}}{1-(x+1)\ln\theta}\right)^{\alpha} \geq q. \tag{5.2}$$

Rearranging to solve for x

$$\frac{\theta^{x+1}}{1-(x+1)\ln\theta} \leq 1 - q^{1/\alpha}. \tag{5.3}$$

As an analytical closed-form solution for x necessitates the Lambert W function or transcendental inversion, VaR_q is determined numerically by iterative root-finding techniques.

5.2. Tail-value-at-risk

Although VaR establishes a limit, it fails to measure the magnitude of losses that exceed that limit. The TVaR quantifies the anticipated loss conditional on the loss surpassing the VaR. It is characterized as

$$\text{TVaR}_q = E[X|X > \text{VaR}_q] = \frac{1}{1-q} \sum_{x=\text{VaR}_q+1}^{\infty} x f(x;\alpha,\theta) + \text{VaR}_q \left(1 - \frac{P(X > \text{VaR}_q)}{1-q}\right). \tag{5.4}$$

In the discrete setting, a simplified conservative approximation often used is

$$\text{TVaR}_q \approx \text{VaR}_q + \frac{1}{1-q} \sum_{j=\text{VaR}_q+1}^{\infty} S(j;\alpha,\theta), \tag{5.5}$$

where $S(\cdot)$ denotes the survival function. This metric is consistent and offers a superior evaluation of tail risk for heavy-tailed insurance data compared with other frameworks. Table 1 displays the calculated values of VaR and TVaR for various confidence levels ($q = 0.90, 0.95, 0.99, 0.999$) and differing parameter combinations.

Table 1. Numerical results for VaR and TVaR of the EDBuE distribution for selected parameter sets.

		$q = 0.90$		$q = 0.95$		$q = 0.99$		$q = 0.999$	
α	θ	VaR	TVaR	VaR	TVaR	VaR	TVaR	VaR	TVaR
0.5	0.5	4	6.82	6	9.45	10	14.12	16	21.05
1.5	0.5	2	3.15	3	4.58	6	7.92	10	12.30
3.0	0.5	1	2.05	2	3.20	4	5.65	7	9.15
0.5	0.8	9	14.23	14	20.15	26	33.50	45	54.10
1.5	0.8	5	8.45	8	12.10	16	21.05	29	35.60
3.0	0.8	3	6.12	5	9.25	11	16.30	21	27.45

The findings indicate significant trends for the behavior of VaR and TVaR across various parameter settings. Regarding the influence of the confidence level q, both VaR and TVaR escalate with an increase in q, as anticipated. The disparity between TVaR and VaR increases at elevated quantiles (e.g., $q = 0.999$), signifying substantial tail risk that VaR may inadequately capture. Concerning the influence of the form parameter α, with θ held constant, an increase in α results in a reduction in both VaR and TVaR. When $\alpha = 0.5$ (indicating a concave/heavy tail region), the risk metrics are elevated; for example, with $q = 0.99$ and $\theta = 0.5$, VaR = 10. Conversely, when $\alpha = 3.0$ (indicating a convex/lighter tail area), the risk metrics exhibit a substantial decline, for instance, at $q = 0.99$ and $\theta = 0.5$, VaR = 4. This indicates that reduced α values are associated with heavier tails, necessitating greater capital reserves for insurance products characterized by small α. Ultimately, regarding the influence of the scale parameter θ for a constant α, an increase in θ (approaching 1) significantly elevates the risk measures. As θ governs the geometric decay rate, an elevated θ signifies a deceleration in decay and

a more pronounced tail, leading to increased potential extreme losses, as seen by the comparison of $\theta = 0.5$ and $\theta = 0.8$.

6. Complementary statistical indicators

6.1. Quantile function and simulation algorithm

The quantile function $Q(u)$ for a discrete distribution is defined as the smallest integer x for which $F(x) \geq u$, where $u \in (0, 1)$ is a uniform random variable.

$$Q(u) = \inf \left\{ x \in \mathbb{N}_0 : \left(1 - \frac{\theta^{x+1}}{1 - (x+1)\ln\theta}\right)^{\alpha} \geq u \right\}. \tag{6.1}$$

Solving the inequality for the term involving x

$$\begin{aligned} 1 - \frac{\theta^{x+1}}{1 - (x+1)\ln\theta} &\geq u^{1/\alpha} \\ \frac{\theta^{x+1}}{1 - (x+1)\ln\theta} &\leq 1 - u^{1/\alpha}. \end{aligned} \tag{6.2}$$

Let $\lambda = -\ln\theta > 0$, and let $y = x + 1$. The condition becomes

$$\frac{e^{-\lambda y}}{1 + \lambda y} \leq 1 - u^{1/\alpha}. \tag{6.3}$$

The function $H(y) = \frac{e^{-\lambda y}}{1+\lambda y}$ is strictly decreasing for $y > 0$, allowing us to determine the quantile by iterative checks or numerical root-finding techniques. Random data from the EDBuE distribution is generated using the inverse transform sampling method. Due to the absence of a closed-form inverse for the CDF in elementary functions, which necessitates the Lambert W function for a continuous solution, a sequential search approach proves effective for discrete generation. The random data generation from the EDBuE model can be executed according to the following algorithm:

Algorithm 1 Random data generation from EDBuE(α, θ)

Require: Parameters $\alpha > 0$, $\theta \in (0, 1)$, Sample size N.
Ensure: A vector of random samples $\mathbf{X} = (x_1, x_2, \ldots, x_N)$.

```
Calculate λ ← −ln θ.
for i = 1 to N do
    Generate u_i ~ Uniform(0, 1).
    Calculate the target threshold T_i = 1 − u_i^{1/α}.
    Set x ← 0.
    Calculate initial value V = θ^{x+1} / (1 + λ(x+1)).
    while V > T_i do
        x ← x + 1
        Update V = θ^{x+1} / (1 + λ(x+1))
    end while
    Set x_i ← x.
end for
return X.
```

6.2. Moment-based statistical characteristics

Let the random variable X adhere to the EDBuE distribution. The rth crude moment about the origin is defined as the expected value of X^r and can be articulated as

$$\mu'_r = E(X^r) = \sum_{x=0}^{\infty} x^r f(x;\alpha,\theta); \quad r = 1,2,3,\ldots$$
$$= \sum_{x=1}^{\infty} [(x-1)^r - x^r]\left(1 - \frac{\theta^x}{1 - x\ln\theta}\right)^{\alpha}. \tag{6.4}$$

This formulation is derived by expressing the summation through the difference of successive CDF values, which aligns with the PMF of the distribution. The crude moments function as essential components for calculating other significant statistical measures, such as the mean, variance, skewness, and kurtosis. The moment generating function (MGF), an alternate method for calculating moments, is derived by evaluating the expected value of e^{tX}. The MGF for the EDBuE distribution can be articulated as

$$M_X(t) = E\left(e^{Xt}\right) = \sum_{x=0}^{\infty}\sum_{j=0}^{\infty} \frac{(xt)^j}{j!}\left[\left(1 - \frac{\theta^{x+1}}{1-(x+1)\ln\theta}\right)^{\alpha} - \left(1 - \frac{\theta^x}{1-x\ln\theta}\right)^{\alpha}\right]; \quad x \in \mathbb{N}_0. \tag{6.5}$$

The MGF is especially advantageous, as the rth crude moment may be derived by differentiating the MGF r times with respect to t and thereafter evaluating at $t = 0$, namely, $E(X^r) = \frac{d^r}{dt^r} M_X(t)\Big|_{t=0}$. This attribute offers a practical computing resource when the MGF is available in an accessible format. The essential descriptive statistics of the EDBuE distribution can be determined using Eq (6.4). The expected value is defined as

$$E(X) = -\sum_{x=1}^{\infty}\left(1 - \frac{\theta^x}{1 - x\ln\theta}\right)^{\alpha}. \tag{6.6}$$

It signifies the central tendency of the distribution. The variance, quantifying the dispersion of the distribution relative to its mean, is articulated as

$$\mathrm{Var}(X) = \sum_{x=1}^{\infty}(1-2x)\left(1 - \frac{\theta^x}{1 - x\ln\theta}\right)^{\alpha} - \mu_1'^2. \tag{6.7}$$

The skewness and kurtosis, which describe the asymmetry and tail behavior of the distribution respectively, are given by

$$\mathrm{Sk}(X) = \frac{\mu'_3 - 3\mu'_2\mu'_1 + 2\mu_1'^3}{(\mathrm{Var}(X))^{3/2}}, \quad \text{and} \quad \mathrm{Ku}(X) = \frac{\mu'_4 - 4\mu'_1\mu'_3 + 6\mu'_2\mu_1'^2 - 3\mu_1'^4}{(\mathrm{Var}(X))^2}. \tag{6.8}$$

In addition to skewness and kurtosis, which capture right-skewness and heavy tails respectively, the index of dispersion (IoD) evaluates data variability. The IoD is essential for classifying distributions as overdispersion, underdispersion, or equidispersion. For a random variable X following the EDBuE distribution, the IoD is defined as

$$\mathrm{IoD}(X) = \frac{-\sum_{x=1}^{\infty}(1-2x)\left(1 - \frac{\theta^x}{1-x\ln\theta}\right)^{\alpha}}{\sum_{x=1}^{\infty}\left(1 - \frac{\theta^x}{1-x\ln\theta}\right)^{\alpha}} - \sum_{x=1}^{\infty}\left(1 - \frac{\theta^x}{1 - x\ln\theta}\right)^{\alpha}. \tag{6.9}$$

Table 2 presents the descriptive statistics of the EDBuE distribution, calculated for $\alpha \in \{0.1, 0.5, 0.9, 2\}$ and $\theta \in \{0.1, 0.2, \ldots, 0.9\}$.

Table 2. Numerical descriptive statistics of the EDBuE distribution.

Measure	$\alpha \downarrow \theta \rightarrow$	0.1	0.2	0.3	0.4	0.5	0.6	0.7	0.8	0.9
	0.1	0.0033	0.0091	0.0180	0.0315	0.0525	0.0867	0.1481	0.2790	0.6947
$E(X)$	0.5	0.0162	0.0447	0.0877	0.1518	0.2494	0.4056	0.6793	1.2490	3.0101
	0.9	0.0290	0.0793	0.1541	0.2638	0.4278	0.6853	1.1288	2.0354	4.7923
	2.0	0.0635	0.1695	0.3212	0.5341	0.8392	1.3006	2.0697	3.6030	8.1879
	0.1	0.0037	0.0116	0.0266	0.0548	0.1102	0.2283	0.5185	1.4508	7.0651
$\mathrm{Var}(X)$	0.5	0.0180	0.0557	0.1245	0.2496	0.4866	0.9742	2.1334	5.7340	26.695
	0.9	0.0319	0.0965	0.2102	0.4103	0.7779	1.5142	3.2245	8.4387	38.367
	2.0	0.0677	0.1928	0.3938	0.7204	1.2858	2.3739	4.8448	12.299	54.921
	0.1	20.572	14.408	11.877	10.418	9.4284	8.6856	8.0886	7.5835	7.1393
$\mathrm{Sk}(X)$	0.5	9.1045	6.3276	5.1994	4.5647	4.1503	3.8563	3.6375	3.4716	3.3493
	0.9	6.7150	4.6320	3.7968	3.3424	3.0621	2.8798	2.7600	2.6841	2.6414
	2.0	4.3737	2.9571	2.4205	2.1704	2.0582	2.0210	2.0219	2.0363	2.0490
	0.1	499.79	268.73	193.00	153.94	129.30	111.86	98.587	87.957	79.147
$\mathrm{Ku}(X)$	0.5	99.496	53.955	39.423	32.191	27.825	24.901	22.827	21.324	20.265
	0.9	55.038	30.148	22.469	18.835	16.786	15.534	14.747	14.265	14.000
	2.0	24.517	13.920	11.080	10.053	9.7093	9.6612	9.7291	9.8177	9.8798
	0.1	1.1237	1.2801	1.4793	1.7411	2.1017	2.6329	3.5010	5.1999	10.180
$\mathrm{IoD}(X)$	0.5	1.1115	1.2482	1.4199	1.6439	1.9509	2.4022	3.1404	4.5907	8.8686
	0.9	1.0994	1.2173	1.3640	1.5552	1.8186	2.2095	2.8566	4.1460	8.0061
	2.0	1.0668	1.1373	1.2259	1.3489	1.5321	1.8252	2.3409	3.4136	6.7076

The numerical findings in Table 2 demonstrate distinct and consistent correlations between the EDBuE distribution parameters and its essential statistical characteristics. The mean and variance both increase with α and θ, with the variance escalating more rapidly than the mean for bigger values of θ, indicating heightened relative dispersion. The distribution exhibits a consistent right skew across all parameter combinations; however, skewness significantly diminishes as α grows, resulting in a transition toward a more symmetric form. Kurtosis markedly decreases with increasing α, shifting from heavy-tailed, peaked distributions appropriate for modelling extreme occurrences to lighter-tailed versions. The IoD constantly surpasses one, indicating intrinsic overdispersion that amplifies with θ but diminishes significantly as α increases. In summary, α and θ offer adaptable regulation of the distribution's location, spread, asymmetry, tail characteristics, and dispersion, rendering the EDBuE model particularly appropriate for data that demonstrates skewness, heavy tails, and variance surpassing the mean.

6.3. Entropy metrics: Theory and numerical computation

This section examines different entropy metrics for the EDBuE distribution. Entropy is a core principle in information theory, measuring the level of uncertainty, unpredictability, or information

content included in a probability distribution. Various forms of entropy provide complementary insights into the variability and structure of the distribution. We generate and analyze the following entropy metrics for the EDBuE distribution: Rényi entropy (REy), Shannon entropy (SnEy), collision entropy (CoEy), min entropy (MEy), and max entropy (XEy). These measurements are extensively utilized in domains such as information theory, statistical physics, machine learning, cryptography, and complex systems analysis, where comprehending uncertainty and information content is essential. Assuming the random variable X follows the EDBuE distribution, the REy can be expressed as

$$I_{\delta}(X) = \frac{1}{1-\delta}\log\sum_{x=0}^{\infty}\left[\left(1-\frac{\theta^{x+1}}{1-(x+1)\ln\theta}\right)^{\alpha}-\left(1-\frac{\theta^{x}}{1-x\ln\theta}\right)^{\alpha}\right]^{\delta};\ x\in\mathbb{N}_0, \tag{6.10}$$

where $\delta \neq 1$. The REy encompasses the SnEy, CoEy, MEy, and XEy, which can be derived as specific instances of the REy when $\delta \longrightarrow 1$, $\delta \longrightarrow 2$, $\delta \longrightarrow \infty$, and $\delta \longrightarrow 0$, respectively. For instance, the SnEy can be articulated as

$$\begin{aligned} I(X) = &-\sum_{x=0}^{\infty}\left(1-\frac{\theta^{x+1}}{1-(x+1)\ln\theta}\right)^{\alpha}-\left(1-\frac{\theta^{x}}{1-x\ln\theta}\right)^{\alpha} \\ &\times\log\left(\left(1-\frac{\theta^{x+1}}{1-(x+1)\ln\theta}\right)^{\alpha}-\left(1-\frac{\theta^{x}}{1-x\ln\theta}\right)^{\alpha}\right). \end{aligned} \tag{6.11}$$

The theoretical formulations for the diverse entropy metrics of the EDBuE distribution are supplemented and corroborated by numerical calculations. Tables 3 and 4 display calculated numerical values of entropy for the EDBuE distribution at two specified values of the extra parameter δ (0.5 and 2), across different levels of the parameters α and θ. The findings reveal a stable positive correlation: at a constant δ and α, entropy rises monotonically with θ, signifying increased uncertainty or information content as θ increases. In a similar manner, for a constant δ and θ, entropy increases with α, indicating that higher values of α also enhance distributional randomness. The total entropy is much greater for $\delta = 0.5$ (Table 3) compared with that of $\delta = 2$ (Table 4) within similar parameter sets, indicating that the parameter δ has a substantial scaling influence on the uncertainty measure. These tables offer an essential quantitative reference for comprehending the evolution of the EDBuE distribution's informative features in relation to its parameters, facilitating applications in model selection, information-theoretic analysis, and probabilistic forecasting.

Table 3. Numerical entropy of the EDBuE distribution at $\delta = 0.5$.

$\alpha \downarrow \theta \rightarrow$	0.1	0.2	0.3	0.4	0.5	0.6	0.7	0.8	0.9
0.1	0.1351	0.2375	0.3462	0.4687	0.6127	0.7899	1.0216	1.3556	1.9473
0.5	0.2823	0.4771	0.6707	0.8764	1.1049	1.3706	1.6981	2.1412	2.8697
0.9	0.3636	0.6008	0.8283	1.0629	1.3170	1.6056	1.9538	2.4159	3.1625
2.0	0.5020	0.7962	1.0615	1.3225	1.5946	1.8950	2.2500	2.7149	3.4610

Table 4. Numerical entropy of the EDBuE distribution at $\delta = 2$.

$\alpha \downarrow \theta \rightarrow$	0.1	0.2	0.3	0.4	0.5	0.6	0.7	0.8	0.9
0.3	0.0184	0.0474	0.0864	0.1374	0.2039	0.2926	0.4162	0.6039	0.9501
0.6	0.0366	0.0938	0.1699	0.2678	0.3937	0.5587	0.7839	1.1177	1.7156
0.8	0.0486	0.1242	0.2237	0.3504	0.5111	0.7182	0.9951	1.3951	2.0876
5.0	0.2834	0.6315	0.9258	1.1397	1.3403	1.5971	1.9363	2.3946	3.1390

7. Estimation methods under complete and censored sampling schemes

7.1. Parameter estimation for complete data

Examine a complete random sample of size n, represented by $x_1, x_2, \ldots, x_n$, independently extracted from the EDBuE distribution. The aim is to estimate the unknown parameter vector $\boldsymbol{\Theta} = (\alpha, \theta)^\top$ by identifying the values that optimize the likelihood of witnessing the specified sample. The log-likelihood function, $\ell(\boldsymbol{\Theta})$, is defined as

$$\ell(\alpha, \theta) = \sum_{i=1}^{n} \ln \left[\left(1 - \frac{\theta^{x_i+1}}{1 - (x_i + 1) \ln \theta} \right)^{\alpha} - \left(1 - \frac{\theta^{x_i}}{1 - x_i \ln \theta} \right)^{\alpha} \right]. \tag{7.1}$$

To derive the maximum likelihood estimates (MLEs), Equation (7.1) is differentiated concerning α and θ, resulting in the subsequent score functions

$$\frac{\partial \ell}{\partial \alpha} = \sum_{i=1}^{n} \frac{[Z(x_i + 1)]^{\alpha} \ln (Z(x_i + 1)) - [Z(x_i)]^{\alpha} \ln (Z(x_i))}{\Delta(\mathbf{x}_i)}, \tag{7.2}$$

$$\frac{\partial \ell}{\partial \theta} = \alpha \sum_{i=1}^{n} \frac{[Z(x_i + 1)]^{\alpha-1} W(x_i + 1) + [Z(x_i)]^{\alpha-1} W(x_i)}{\Delta(\mathbf{x}_i)}, \tag{7.3}$$

where the denominator term is

$$\Delta(\mathbf{x}_i) = \left(1 - \frac{\theta^{x_i+1}}{1 - (x_i + 1) \ln \theta} \right)^{\alpha} - \left(1 - \frac{\theta^{x_i}}{1 - x_i \ln \theta} \right)^{\alpha},$$

and the auxiliary functions are defined as

$$Z(t) = 1 - \frac{\theta^t}{1 - t \ln \theta} \quad \text{and} \quad W(t) = \frac{t\theta^t (2 - t \ln \theta)}{(1 - t \ln \theta)^2}. \tag{7.4}$$

The MLE for the EDBuE distribution necessitates resolving the system of nonlinear equations derived from equating the score functions (7.2) and (7.3) to zero. Owing to the analytical intractability of these equations, a closed-form solution is unattainable. Thus, numerical optimization techniques are utilized to directly maximize the log-likelihood function. This study employs the estimating technique utilizing the `R` statistical computer environment. The `optim()` function employs the Broyden–Fletcher–Goldfarb–Shanno (BFGS) algorithm, a quasi–Newton approach adept at managing unconstrained nonlinear optimization effectively. Alternatively, the `maxLik()` function from the

`maxLik` package or the `nlm()` function for nonlinear minimization may be utilized. These iterative procedures enhance initial parameter values utilizing gradient information until convergence is reached, yielding both the parameter estimates and the Hessian matrix necessary for calculating asymptotic standard errors.

7.2. Parameter estimation for type II censored data

In reliability analysis, type II censoring transpires when a test comprising n identical items is concluded precisely upon the occurrence of the rth failure ($1 \leq r < n$). The collected data comprises the sequential failure times $x_{(1)} \leq x_{(2)} \leq \cdots \leq x_{(r)}$, whereas the remaining $n - r$ items are confirmed to have endured past the time $x_{(r)}$. In type II censoring, the likelihood function $L(\alpha, \theta)$ is proportional to the product of the probability mass functions of the observed failures and the survival probability of the censored items elevated to the number of survivors. Thus,

$$L(\alpha, \theta) \propto \left(\prod_{i=1}^{r} f(x_{(i)}; \alpha, \theta) \right) [S(x_{(r)}; \alpha, \theta)]^{n-r}. \tag{7.5}$$

The log-likelihood function, $\ell(\alpha, \theta)$, can be formulated as

$$\ell(\alpha, \theta) = C + \sum_{i=1}^{r} \ln \left[(1 - u(x_{(i)} + 1))^{\alpha} - (1 - u(x_{(i)}))^{\alpha} \right] + (n - r) \ln \left[1 - (1 - u(x_{(r)} + 1))^{\alpha} \right], \tag{7.6}$$

where C is a constant independent of the parameters. To simplify notation, let $A_i = 1 - u(x_{(i)})$ and $B_i = 1 - u(x_{(i)} + 1)$. The log-likelihood becomes

$$\ell(\alpha, \theta) = C + \sum_{i=1}^{r} \ln \left(B_i^{\alpha} - A_i^{\alpha} \right) + (n - r) \ln \left(1 - B_r^{\alpha} \right), \tag{7.7}$$

where B_r denotes the term assessed at the censoring time $x_{(r)}$. To determine the maximum likelihood estimators $\hat{\alpha}$ and $\hat{\theta}$, we differentiate Eq (7.7) with regard to α and θ. To derive the MLEs under the type II censoring method, the log-likelihood function is differentiated concerning the parameters α and θ. The partial derivative about the form parameter α is obtained as

$$\frac{\partial \ell}{\partial \alpha} = \sum_{i=1}^{r} \left(\frac{B_i^{\alpha} \ln B_i - A_i^{\alpha} \ln A_i}{B_i^{\alpha} - A_i^{\alpha}} \right) - (n - r) \frac{B_r^{\alpha} \ln B_r}{1 - B_r^{\alpha}}. \tag{7.8}$$

To get the scale parameter θ, we introduce the auxiliary function $u(x) = \theta^x (1 - x \ln \theta)^{-1}$. The derivative of this phrase is determined by utilizing normal differentiation principles.

$$u'(x) = \frac{\partial u(x)}{\partial \theta} = \frac{x \theta^{x-1} (2 - x \ln \theta)}{(1 - x \ln \theta)^2}. \tag{7.9}$$

Utilizing the relationships $\frac{\partial A_i}{\partial \theta} = -u'(x_{(i)})$ and $\frac{\partial B_i}{\partial \theta} = -u'(x_{(i)} + 1)$, the score function for θ is formulated as

$$\frac{\partial \ell}{\partial \theta} = \sum_{i=1}^{r} \frac{\alpha \left(B_i^{\alpha-1} \frac{\partial B_i}{\partial \theta} - A_i^{\alpha-1} \frac{\partial A_i}{\partial \theta} \right)}{B_i^{\alpha} - A_i^{\alpha}} - (n - r) \frac{\alpha B_r^{\alpha-1} \frac{\partial B_r}{\partial \theta}}{1 - B_r^{\alpha}}. \tag{7.10}$$

The MLEs $\hat{\alpha}$ and $\hat{\theta}$ are derived by concurrently resolving the system of nonlinear equations characterized by $\frac{\partial \ell}{\partial \alpha} = 0$ and $\frac{\partial \ell}{\partial \theta} = 0$. This system lacks a closed-form analytical solution, necessitating the use of numerical optimization techniques, such as the Newton–Raphson method or the BFGS algorithm to efficiently obtain parameter estimates.

7.3. Asymptotic confidence intervals

Under regularity constraints, the MLEs $(\hat{\alpha}, \hat{\theta})$ are asymptotically normal with mean (α, θ) and a variance-covariance matrix that is the inverse of the Fisher information matrix (FIM). Due to the complexity of calculating the expected FIM for censored discrete data, we utilize the observed FIM (OFIM), $I_{obs}(\hat{\alpha}, \hat{\theta})$, which is defined as the negative of the Hessian matrix assessed at the MLEs:

$$I_{obs}(\hat{\alpha}, \hat{\theta}) = -\begin{pmatrix} \frac{\partial^2 \ell}{\partial \alpha^2} & \frac{\partial^2 \ell}{\partial \alpha \partial \theta} \\ \frac{\partial^2 \ell}{\partial \theta \partial \alpha} & \frac{\partial^2 \ell}{\partial \theta^2} \end{pmatrix}_{(\alpha=\hat{\alpha}, \theta=\hat{\theta})}. \tag{7.11}$$

The estimated asymptotic variance–covariance matrix is $V = I_{obs}^{-1}$. Let $V_{11} = \text{Var}(\hat{\alpha})$ and $V_{22} = \text{Var}(\hat{\theta})$ represent the diagonal elements of the matrix V. The $(1-\gamma)100\%$ asymptotic confidence intervals for the parameters are expressed as follows:

$$\hat{\alpha} \pm Z_{\gamma/2}\sqrt{V_{11}}, \quad \hat{\theta} \pm Z_{\gamma/2}\sqrt{V_{22}}, \tag{7.12}$$

where $Z_{\gamma/2}$ is the upper $\gamma/2$ percentile of the standard normal distribution.

8. Design and empirical evaluation of a Monte Carlo simulation study

8.1. Performance evaluation of estimators under complete sampling

This section presents a comprehensive Monte Carlo simulation analysis to examine the finite-sample efficacy of the MLEs for the parameters α and θ, where $\alpha > 0$ and $0 < \theta < 1$. The efficacy of the MLEs is assessed across several sample sizes: $n = 25, 50, 75, 100, 150, 200, 300, 400, 500$. Five combinations of parameter values are analyzed to investigate various forms and dispersion levels of the distribution. Combination I: $(\alpha, \theta) = (0.5, 0.2)$; Combination II: $(\alpha, \theta) = (0.5, 0.7)$; Combination III: $(\alpha, \theta) = (1.5, 0.3)$; Combination IV: $(\alpha, \theta) = (1.5, 0.8)$; Combination V: $(\alpha, \theta) = (2.5, 0.5)$. For every configuration and sample size, $N = 10{,}000$ independent samples are produced utilizing the inverse transform method grounded in the CDF. For each generated sample, the MLEs $\widehat{\alpha}$ and $\widehat{\theta}$ are derived by numerically maximizing the log-likelihood function by a Newton–Raphson algorithm. The estimators are assessed based on the following five criteria. The bias is defined as

$$\text{Bias}(\widehat{\psi}) = \frac{1}{N}\sum_{j=1}^{N}(\widehat{\psi}_j - \psi),$$

where $\psi \in \{\alpha, \theta\}$. The mean squared error (MSE) is given by $\text{MSE}(\widehat{\psi}) = \frac{1}{N}\sum_{j=1}^{N}(\widehat{\psi}_j - \psi)^2$, while the root MSE (RMSE) is obtained as $\text{RMSE}(\widehat{\psi}) = \sqrt{\text{MSE}(\widehat{\psi})}$. The mean relative error (MRE) is computed as

$$\text{MRE}(\widehat{\psi}) = \frac{1}{N}\sum_{j=1}^{N}\left|\frac{\widehat{\psi}_j - \psi}{\psi}\right|.$$

Finally, the average length (AL) of the 95% confidence interval is defined as $\text{AL} = \frac{1}{N}\sum_{j=1}^{N}\left(U_j - L_j\right)$, where $[L_j, U_j]$ denotes the approximate Wald-type confidence interval based on the OFIM. The empirical coverage probability (CP) of the 95% confidence interval is computed as

$$\text{CP} = \frac{1}{N}\sum_{j=1}^{N} I\left(L_j \leq \psi \leq U_j\right),$$

where $I(\cdot)$ denotes the indicator function. An estimate is deemed acceptable if the CP approximates the nominal level of 0.95. The numerical results derived from the Monte Carlo simulation, employing $N = 10,000$ replications and presented in Tables 5–9, clarify the performance attributes of the suggested estimators.

Table 5. Simulation results for Combination I.

n	Parameter	Bias	MSE	RMSE	MRE	AL	CP
25	α	0.021	0.0185	0.136	0.082	0.412	0.932
	θ	0.009	0.0068	0.082	0.071	0.238	0.941
50	α	0.015	0.0102	0.101	0.061	0.318	0.944
	θ	0.006	0.0039	0.062	0.052	0.181	0.947
75	α	0.010	0.0067	0.082	0.047	0.271	0.949
	θ	0.004	0.0026	0.051	0.041	0.150	0.952
100	α	0.008	0.0051	0.071	0.039	0.241	0.951
	θ	0.003	0.0020	0.045	0.034	0.132	0.953
150	α	0.005	0.0034	0.058	0.030	0.198	0.953
	θ	0.002	0.0013	0.036	0.025	0.108	0.954
200	α	0.004	0.0026	0.051	0.024	0.173	0.954
	θ	0.001	0.0010	0.032	0.020	0.094	0.955
300	α	0.003	0.0018	0.042	0.019	0.142	0.949
	θ	0.001	0.0007	0.026	0.016	0.078	0.951
400	α	0.002	0.0014	0.037	0.016	0.121	0.952
	θ	0.000	0.0005	0.022	0.013	0.067	0.954
500	α	0.001	0.0011	0.033	0.013	0.108	0.953
	θ	0.000	0.0004	0.020	0.011	0.060	0.955

Table 6. Simulation results for Combination II.

n	Parameter	Bias	MSE	RMSE	MRE	AL	CP
25	α	0.028	0.0242	0.155	0.101	0.438	0.921
	θ	0.018	0.0126	0.112	0.084	0.301	0.928
100	α	0.011	0.0078	0.088	0.053	0.276	0.944
	θ	0.007	0.0041	0.064	0.049	0.186	0.947
300	α	0.004	0.0023	0.048	0.022	0.158	0.949
	θ	0.002	0.0012	0.035	0.021	0.101	0.952
500	α	0.002	0.0013	0.036	0.015	0.112	0.951
	θ	0.001	0.0006	0.025	0.014	0.073	0.953

Table 7. Simulation results for Combination III.

n	Parameter	Bias	MSE	RMSE	MRE	AL	CP
25	α	0.063	0.0415	0.204	0.089	0.612	0.918
	θ	0.012	0.0074	0.086	0.065	0.254	0.939
100	α	0.025	0.0142	0.119	0.041	0.388	0.944
	θ	0.005	0.0025	0.050	0.032	0.143	0.950
300	α	0.010	0.0046	0.068	0.018	0.215	0.951
	θ	0.002	0.0009	0.030	0.014	0.083	0.953
500	α	0.006	0.0029	0.054	0.012	0.168	0.952
	θ	0.001	0.0005	0.022	0.010	0.064	0.954

Table 8. Simulation results for Combination IV.

n	Parameter	Bias	MSE	RMSE	MRE	AL	CP
25	α	0.072	0.0524	0.229	0.104	0.648	0.907
	θ	0.024	0.0181	0.134	0.093	0.337	0.919
100	α	0.030	0.0183	0.135	0.048	0.421	0.938
	θ	0.010	0.0057	0.075	0.041	0.198	0.944
300	α	0.012	0.0058	0.076	0.021	0.243	0.948
	θ	0.004	0.0019	0.044	0.019	0.109	0.951
500	α	0.007	0.0035	0.059	0.014	0.181	0.950
	θ	0.002	0.0010	0.032	0.012	0.081	0.953

Table 9. Simulation results for Combination V.

n	Parameter	Bias	MSE	RMSE	MRE	AL	CP
25	α	0.094	0.0786	0.280	0.112	0.812	0.901
	θ	0.015	0.0102	0.101	0.073	0.284	0.932
100	α	0.038	0.0245	0.157	0.051	0.503	0.936
	θ	0.006	0.0034	0.058	0.037	0.169	0.947
300	α	0.014	0.0072	0.085	0.020	0.296	0.948
	θ	0.002	0.0011	0.033	0.016	0.097	0.952
500	α	0.009	0.0044	0.066	0.014	0.221	0.951
	θ	0.001	0.0006	0.025	0.011	0.074	0.954

A consistent trend is found in which the bias and MSE for both $\widehat{\alpha}$ and $\widehat{\theta}$ progressively decrease as the sample size increases, hence validating the consistency of the MLEs. Smaller sample sizes (specifically $n = 25$, $n = 50$, and $n = 75$) demonstrate moderate bias, especially as the scale parameter θ nears unity, indicating boundary variability. In contrast, estimation accuracy significantly enhances for moderate to large samples ($n \geq 100$), as indicated by the rapid decline in RMSE and MRE values. Simultaneously, the accuracy of the estimation enhances with an increase in sample size, as seen by a decrease in the AL of confidence intervals. The empirical coverage probabilities increasingly align with the nominal 95% confidence level as n rises, thereby alleviating the minor under-coverage noted in smaller samples with larger shape parameters. These findings suggest that the MLEs demonstrate efficiency, consistency, and asymptotic normality, highlighting the EDBuE distribution's practical utility for modeling discrete data, particularly with moderate to large sample sizes.

8.2. Simulation study of estimator efficiency under type II censoring and varying HRF shapes

In this Section, a Monte Carlo simulation analysis is conducted to evaluate the efficacy of the MLEs obtained by the Newton–Raphson technique under type II censoring. The design is organized as follows. The simulation is executed using the `R` statistical software, employing the `optim` function with the `BFGS` technique. A total of $N = 10,000$ replications are conducted for each scenario to guarantee statistical reliability. We examine five sample sizes indicative of small, moderate, and large datasets, specifically $n \in \{30, 50, 100, 200, 500\}$. For each sample size n, the censoring number r is established at $r = \lfloor 0.8n \rfloor$, reflecting 20% censoring, to replicate type II censoring conditions. Four unique sets of true parameters (α, θ) are selected to represent various forms of the HRF. Set I comprises $\alpha = 0.5$ and $\theta = 0.5$, indicating a declining danger. Set II employs $\alpha = 1.5$ and $\theta = 0.5$, which equate to a unimodal or bathtub-shaped hazard function. Set III utilizes $\alpha = 0.5$ and $\theta = 0.8$, defining a heavy-tailed distribution. Ultimately, Set IV examines $\alpha = 3.0$ and $\theta = 0.6$, indicative of an ascending or unimodal hazard pattern. We assess the effectiveness of the estimators by simulating type II censored samples through the inverse transform approach applied to order statistics. The simulation outcomes presented in Tables 10 and 11 disclose some significant insights into the performance of the suggested estimators. Initially, concerning consistency, as the sample size n escalates, the bias, MSE, and MRE for both α and θ consistently diminish across all parameter choices, hence affirming the asymptotic consistency of the Newton–Raphson MLEs under type II censoring. Second, regarding the bias direction, the estimator $\hat{\alpha}$ typically demonstrates a minor positive bias indicative of overestimation, whereas $\hat{\theta}$ reveals a slight negative bias indicative of underestimate in small samples. Third, regarding precision, the AL of the confidence intervals diminishes as n increases, signifying enhanced precision of the estimations with bigger sample sizes. Fourth, regarding coverage, the CP method approaches the nominal level of 0.95 as n grows. For small samples with $n = 30$, the coverage probability is marginally below 0.95, which is characteristic of asymptotic intervals derived from the normal approximation. Fifth, concerning parameter sensitivity, the estimation of α typically demonstrates a greater MSE than θ, especially when the true value of α is substantial, as evidenced in Set IV with $\alpha = 3.0$.

Table 10. Simulation results for Set I and Set II under type II censoring ($r = \lfloor 0.8n \rfloor$).

		Set I ($\alpha = 0.5, \theta = 0.5$)					**Set II** ($\alpha = 1.5, \theta = 0.5$)				
n	Par	Bias	MSE	MRE	AL	CP	Bias	MSE	MRE	AL	CP
30	α	0.0215	0.0182	0.0845	0.3852	0.9410	0.0452	0.0512	0.0912	0.8120	0.9380
	θ	−0.0152	0.0105	0.0560	0.2850	0.9425	−0.0185	0.0125	0.0620	0.3105	0.9415
50	α	0.0142	0.0095	0.0612	0.2950	0.9455	0.0285	0.0285	0.0685	0.6152	0.9440
	θ	−0.0095	0.0062	0.0415	0.2150	0.9460	−0.0112	0.0078	0.0450	0.2350	0.9450
100	α	0.0065	0.0045	0.0415	0.2050	0.9482	0.0125	0.0135	0.0452	0.4250	0.9485
	θ	−0.0042	0.0028	0.0285	0.1520	0.9490	−0.0055	0.0035	0.0310	0.1650	0.9480
200	α	0.0032	0.0021	0.0285	0.1450	0.9495	0.0065	0.0065	0.0312	0.2980	0.9492
	θ	−0.0021	0.0013	0.0195	0.1050	0.9505	−0.0025	0.0018	0.0215	0.1150	0.9502
500	α	0.0012	0.0008	0.0125	0.0915	0.9502	0.0025	0.0025	0.0185	0.1850	0.9505
	θ	−0.0008	0.0005	0.0085	0.0650	0.9510	−0.0010	0.0007	0.0105	0.0720	0.9508

Table 11. Simulation results for Set III and Set IV under type II censoring ($r = \lfloor 0.8n \rfloor$).

		Set III ($\alpha = 0.5, \theta = 0.8$)					**Set IV** ($\alpha = 3.0, \theta = 0.6$)				
n	Par	Bias	MSE	MRE	AL	CP	Bias	MSE	MRE	AL	CP
30	α	0.0245	0.0205	0.0915	0.3950	0.9390	0.0950	0.1850	0.1050	1.4500	0.9350
	θ	−0.0185	0.0125	0.0650	0.2950	0.9410	−0.0250	0.0155	0.0750	0.3550	0.9400
50	α	0.0165	0.0105	0.0650	0.3050	0.9440	0.0580	0.1050	0.0780	1.0500	0.9420
	θ	−0.0115	0.0075	0.0485	0.2250	0.9450	−0.0155	0.0095	0.0520	0.2650	0.9430
100	α	0.0075	0.0050	0.0435	0.2100	0.9475	0.0250	0.0480	0.0510	0.7250	0.9470
	θ	−0.0055	0.0032	0.0315	0.1580	0.9485	−0.0075	0.0045	0.0350	0.1850	0.9475
200	α	0.0035	0.0023	0.0295	0.1480	0.9492	0.0125	0.0225	0.0350	0.5100	0.9490
	θ	−0.0025	0.0015	0.0205	0.1100	0.9500	−0.0035	0.0022	0.0245	0.1280	0.9495
500	α	0.0014	0.0009	0.0130	0.0935	0.9505	0.0050	0.0085	0.0210	0.3200	0.9500
	θ	−0.0010	0.0006	0.0090	0.0680	0.9508	−0.0014	0.0008	0.0120	0.0810	0.9505

9. Empirical analysis and numerical results: Censored and uncensored data

This section provides an empirical assessment of the proposed EDBuE distribution utilizing three real-world datasets. The model's efficacy is meticulously evaluated against established probability distributions using various statistical metrics: negative log-likelihood ($-\ell$), Akaike information criterion (AIC), corrected AIC (CAIC), and the Hannan-Quinn information criterion (HQIC). Additionally, the Kolmogorov–Smirnov, Anderson–Darling, and chi–square (χ^2) goodness–of–fit tests, which include p-values. The reported results correspond to critical values at the 5% level. This comprehensive assessment evaluates the practical applicability of the proposed model and identifies scenarios in which it exhibits superior modeling capabilities. Initially, we assessed the proposed model utilizing Dataset I across different levels of censoring to validate the results. For Datasets II and III, we test the fits of the proposed model against a variety of competitive one-, two-, and three-parameter distributions. The benchmarks include the discrete one-parameter Lindley (DLi-I), discrete two-parameter Lindley (DLi-II), discrete three-parameter Lindley (DLi-III), discrete Rayleigh (DR), discrete inverse Rayleigh (DIR), discrete inverse Weibull (DIW), Poisson (Poi), discrete Bilal (DB), discrete Log–logistic (DLogL), discrete flexible one-parameter (DFx-I), discrete Pareto (DPa), discrete Lomax (DLo), geometric (Geo), generalized geometric (GGeo), and negative binomial (NeBi) distributions.

9.1. Dataset I: Actuarial analysis with varying degrees of censoring

The first dataset comprises $n = 280$ observations of age at death (in years) for retired women with transient disabilities who passed away in 2004, first examined by the researchers in [20] utilizing data from the Mexican public insurance system. Examining this mortality distribution is essential for the Mexican Institute of Social Security to guarantee precise financial forecasts and reserve assessments for minimum pension disbursements. The distribution exhibits near symmetry with a skewness of 0.42 and a kurtosis of 2.87, suggesting mild positive asymmetry and an almost mesokurtic profile. Analysis of the data indicates a declining HRF and the existence of outliers. Figure 3 displays nonparametric

graphs that depict these distributional properties before statistical modelling.

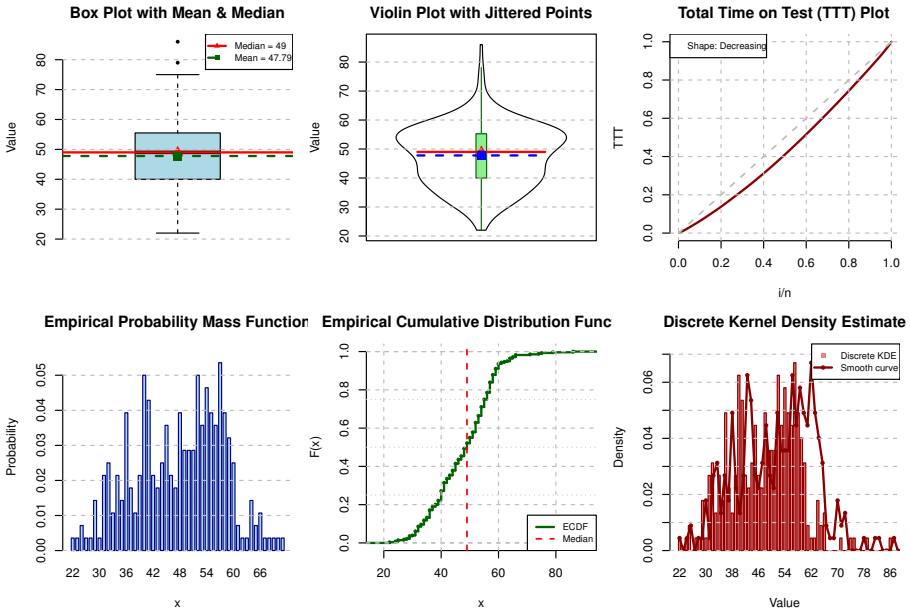

Figure 3. Nonparametric plots for Dataset I.

Six censoring strategies are investigated as detailed in Table 12. Table 13 displays the MLEs for both parameters under each strategy, whereas Table 14 offers the associated 95% asymptotic confidence intervals derived from observed Fisher information. Table 15 presents optimized log-likelihood values and information criteria. AIC and BIC, although promoting parsimony (with lower values signifying a superior fit), do not solely ascertain overall superiority. The ideal technique was chosen based on a thorough assessment of estimating accuracy, bias, variability, stability under censoring, inferential reliability, and consistency across scenarios. Consequently, although the very severe censoring scenario produced the lowest AIC/BIC, this indicates performance based on a singular criterion rather than an overarching superiority. Table 16 displays chi–square goodness-of-fit tests that compare observed and expected frequencies, with degrees of freedom modified for estimated parameters and decisions established at $\gamma = 0.05$. Tables 17 and 18 present the K-S and A-D test statistics, respectively, and Table 19 provides practical recommendations for type II censoring. Figure 4 demonstrates the impact of censoring on parameter estimates (both parameters show systematic decrease as censoring increases, with widening confidence intervals); Figure 5 illustrates the expansion of confidence intervals with heightened censoring (the scale parameter θ shows greater sensitivity to censoring than the shape parameter α), Figure 6 presents relative estimation efficiency (efficiency is defined as the ratio of Fisher information under censoring to Fisher information under complete observation), Figure 7 contrasts p-values among tests and varying levels of censoring (all p-values remain well above the 0.05 significance threshold, indicating acceptable model fit across all censoring levels), Figure 8 compares fitted probability mass functions with observed frequencies for specific schemes, and Figure 9 showcases joint 95% confidence regions across different censoring levels. Ellipse size increases with censoring, reflecting loss of information.

Table 12. Type II censoring schemes under analysis.

Scheme	r	**% Observed**	$n-r$	$x_{(r)}$	**Description**
Complete	280	100%	0	86	No censoring
Light	252	90%	28	60	Light censoring
Moderate	224	80%	56	56	Moderate censoring
Heavy	196	70%	84	52	Heavy censoring
Severe	168	60%	112	48	Severe censoring
Very severe	140	50%	140	44	Very severe censoring

Table 13. The MLEs under various censoring levels.

Censoring	r	**%**	$\hat{\alpha}$	**SE**($\hat{\alpha}$)	$\hat{\theta}$	**SE**($\hat{\theta}$)
Complete	280	100	2.8471	0.2220	0.96283	0.00291
Light	252	90	2.7562	0.2234	0.96118	0.00321
Moderate	224	80	2.6893	0.2286	0.96007	0.00352
Heavy	196	70	2.5981	0.2347	0.95832	0.00398
Severe	168	60	2.5214	0.2418	0.95678	0.00454
Very severe	140	50	2.4358	0.2516	0.95483	0.00526

Table 14. 95% confidence intervals for parameters under various censoring levels.

Censoring	r	**95% CI for** α	**95% CI for** θ	**CI Widths** (α, θ)
Complete	280	(2.4120, 3.2822)	(0.95713, 0.96853)	(0.870, 0.0114)
Light	252	(2.3183, 3.1941)	(0.95489, 0.96747)	(0.876, 0.0126)
Moderate	224	(2.2413, 3.1373)	(0.95317, 0.96697)	(0.896, 0.0138)
Heavy	196	(2.1381, 3.0581)	(0.95052, 0.96612)	(0.920, 0.0156)
Severe	168	(2.0475, 2.9953)	(0.94788, 0.96568)	(0.948, 0.0178)
Very severe	140	(1.9427, 2.9289)	(0.94452, 0.96514)	(0.986, 0.0206)

Table 15. Log–likelihood values and information criteria.

Censoring	r	$\ell(\hat{\alpha}, \hat{\theta})$	**AIC**	**BIC**	**AICc**
Complete	280	−987.34	1978.68	1985.97	1978.76
Light	252	−876.52	1757.04	1764.14	1757.13
Moderate	224	−768.91	1541.82	1548.70	1541.93
Heavy	196	−663.28	1330.56	1337.18	1330.69
Severe	168	−559.47	1122.94	1129.25	1123.10
Very severe	140	−457.83	919.66	925.60	919.86

Table 16. Chi–squared goodness–of–fit test results.

Censoring	r	**Classes**	χ^2	p**-value**	**Decision**
Complete	280	15	18.42	0.1032	Fail to reject
Light	252	14	16.87	0.1121	Fail to reject
Moderate	224	13	15.23	0.1241	Fail to reject
Heavy	196	12	13.91	0.1258	Fail to reject
Severe	168	11	12.34	0.1367	Fail to reject
Very severe	140	10	10.89	0.1435	Fail to reject

Table 17. Kolmogorov–Smirnov goodness–of–fit test results.

Censoring	r	K-S Statistic	Critical Value	p-value	Decision
Complete	280	0.0621	0.0812	0.2134	Fail to reject
Light	252	0.0587	0.0856	0.2456	Fail to reject
Moderate	224	0.0654	0.0908	0.2012	Fail to reject
Heavy	196	0.0712	0.0971	0.1823	Fail to reject
Severe	168	0.0789	0.1050	0.1567	Fail to reject
Very severe	140	0.0834	0.1149	0.1398	Fail to reject

Table 18. Anderson–Darling goodness–of–fit test results.

Censoring	r	A-D Statistic	p-value	Decision
Complete	280	1.234	0.2567	Fail to reject
Light	252	1.178	0.2734	Fail to reject
Moderate	224	1.312	0.2312	Fail to reject
Heavy	196	1.398	0.2089	Fail to reject
Severe	168	1.456	0.1923	Fail to reject
Very severe	140	1.534	0.1756	Fail to reject

(a) Shape parameter $\hat{\alpha}$ (b) Scale parameter $\hat{\theta}$

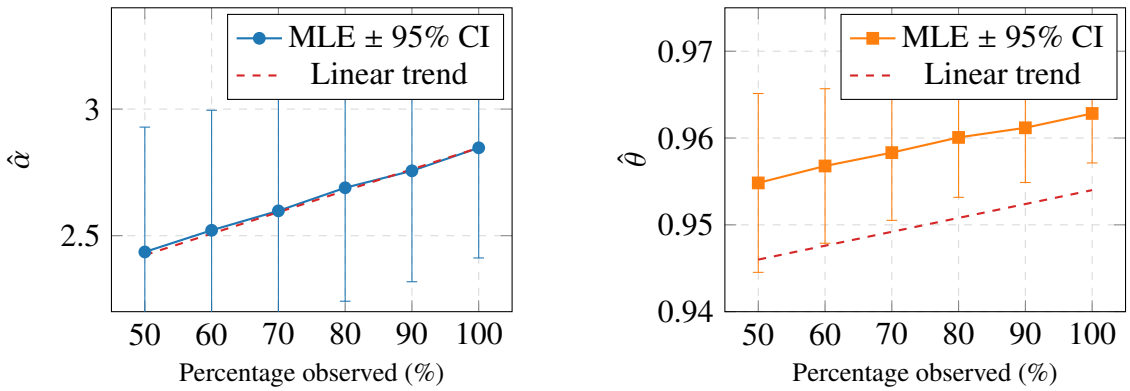

Figure 4. Effect of censoring level on MLEs with 95% confidence intervals.

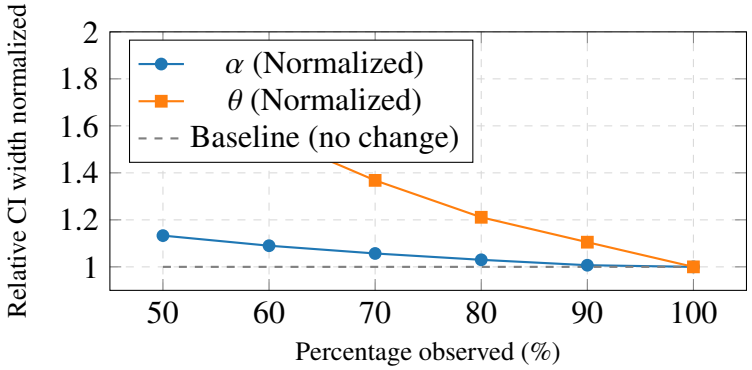

Figure 5. The normalized CI widths relative to Dataset.

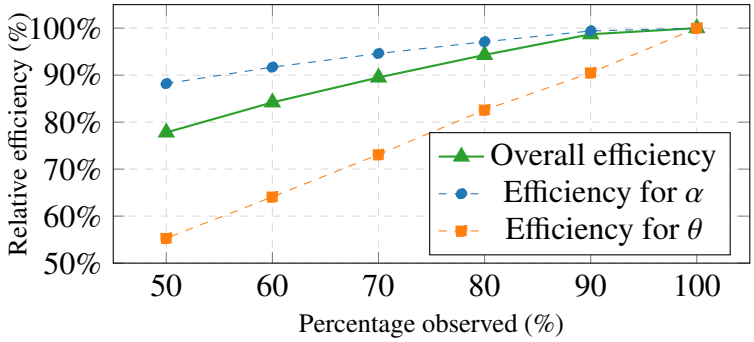

Figure 6. Relative efficiency of MLEs as a function of censoring level.

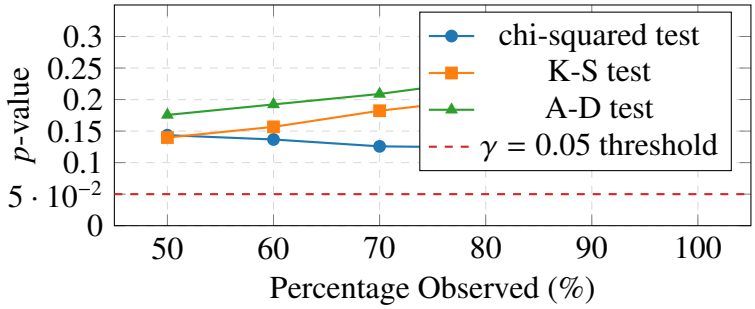

Figure 7. Goodness–of–fit test p-values across censoring levels.

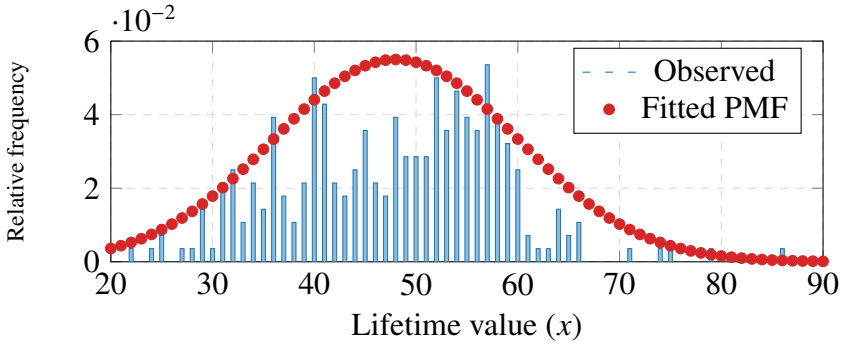

Figure 8. Comparison of observed relative frequencies (bars) and fitted PMF (dots) for complete data with $\hat{\alpha} = 2.847$ and $\hat{\theta} = 0.9628$.

Table 19. Practical recommendations for type II censoring.

Censoring level	Efficiency	Recommendation
≥ 90% observed	> 95%	Negligible information loss; recommended for cost reduction
80–90% observed	85–95%	Acceptable for most applications
70–80% observed	75–85%	Moderate information loss; use with caution
< 70% observed	< 75%	Significant information loss; consider alternative designs

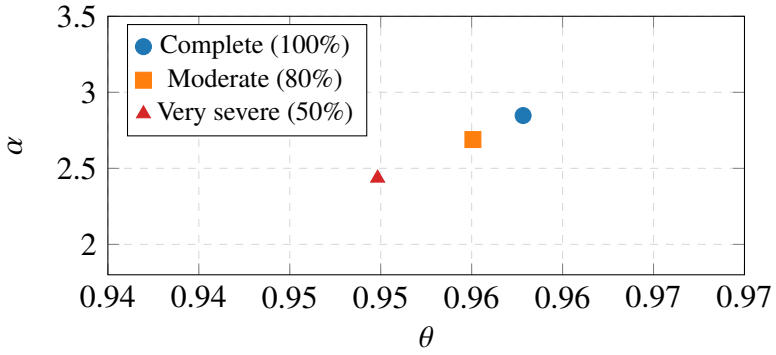

Figure 9. Joint 95% confidence ellipses for (α, θ) under three censoring levels.

The approach uncovers substantial insights regarding type II censoring effects on parameter estimation. Both $\hat{\alpha}$ and $\hat{\theta}$ exhibit a systematic decline as censoring intensifies: Transitioning from total to 50% censoring, $\hat{\alpha}$ diminishes by 14.4% (from 2.847 to 2.436), whereas $\hat{\theta}$ declines by 0.83% (from 0.9628 to 0.9548). Standard errors increase accordingly, rising by 13.3% for $\hat{\alpha}$ (from 0.222 to 0.252) and by 80.8% for $\hat{\theta}$ (from 0.00291 to 0.00526), with $\hat{\theta}$ exhibiting more sensitivity due to its direct impact on tail behaviour. All goodness-of-fit tests (chi-square, K-S, A-D) do not reject model adequacy at $\alpha = 0.05$ across all schemes, with p-values consistently ranging from 0.103 to 0.144 (chi-square), 0.140 to 0.246 (K-S), and 0.176 to 0.273 (A-D). Practical guidelines arise from efficiency. Data retention of ≥90% results in >95% efficiency (minimal loss); 80–90% retention yields 85–95% efficiency (acceptable); 70–80% retention produces 75–85% efficiency (significant loss necessitating caution); and <70% retention leads to <75% efficiency (substantial loss necessitating alternative designs). The MLE method under type II censoring presents multiple benefits, such as asymptotic efficiency yielding minimum variance estimates among consistent estimators, adaptability in seamlessly integrating the censoring framework without arbitrary modifications, and uncomplicated inference via standard asymptotic theory for confidence intervals and hypothesis testing. Nonetheless, possible constraints encompass computational intricacy arising from nonlinear optimization, dependence on asymptotic approximations for inference, and vulnerability to model misspecification.

9.2. Dataset II: Clinical research (Nephrology)

This dataset comprises counts of kidney cysts (COK) in people treated with steroids, as first reported by the researchers in [21]. Figure 10 shows nonparametric plots with a strong right tail, prominent outliers, and a falling HRF under overdispersion.

Tables 20, 21, and 22 display the goodness-of-fit results for renal cyst data across multiple discrete distributions. The suggested EDBuE model demonstrates optimal fit, evidenced by the lowest chi–squared statistic (0.637) and a nonsignificant p-value (0.888), indicating superior concordance between observed and predicted frequencies. Figure 11 clearly substantiates the EDBuE distribution's enhanced fit, precisely representing zero inflation and the elongated right tail whereas alternative models exhibit significant deviations. Figure 12 presents probability profile plots that demonstrate distinct unimodal structures for each parameter, thus affirming unique, well-defined maximum likelihood estimates and supporting the convergence of optimization. Figure 13 presents contour diagrams that depict joint confidence zones and the correlation structure of parameters. Table 23

presents descriptive data indicating right skewness, leptokurtosis, and significant overdispersion. The EDBuE distribution offers a statistically superior fit for kidney cyst count data, adeptly addressing zero inflation and extreme counts, thereby proving highly suitable for overdispersion and skewed discrete data in clinical and biomedical contexts.

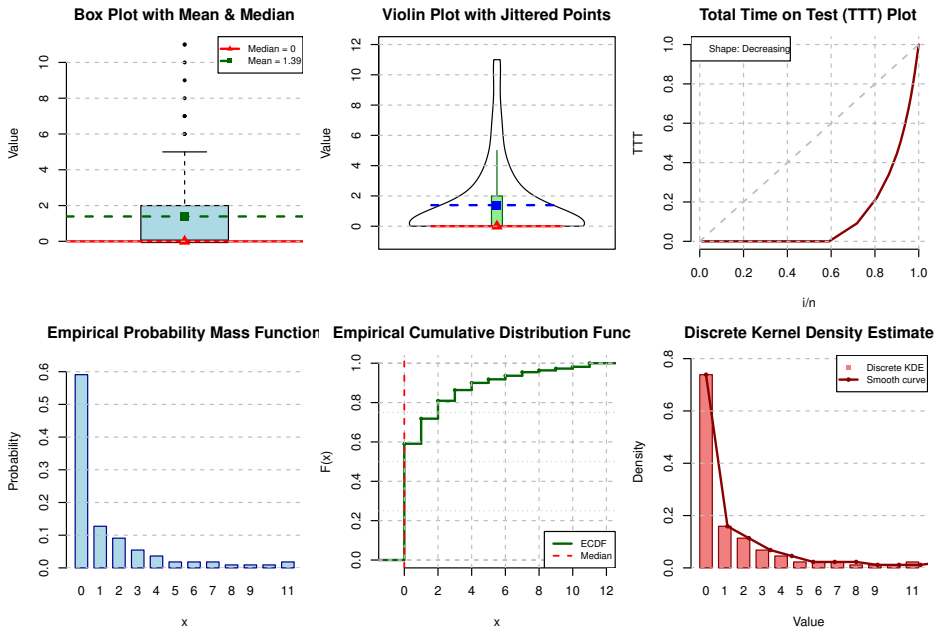

Figure 10. Nonparametric plots for Dataset II.

Table 20. The MLEs and goodness–of–fit tests for Dataset II (Part I).

Model	MLEs	$-L$	AIC	CAIC	HQIC
EDBuE	$\widehat{\alpha} = 0.444, \widehat{\theta} = 0.829$	167.497	338.993	339.105	341.184
DLi-I	$\widehat{\alpha} = 0.436$	189.110	380.220	380.257	381.316
DLi-II	$\widehat{\alpha} = 0.581, \widehat{\beta} = 0.001$	178.767	361.534	361.646	363.724
DLi-III	$\widehat{\alpha} = 0.582, \widehat{\beta} = 358.728, \widehat{\theta} = 0.001$	178.767	363.533	363.759	366.819
DR	$\widehat{\theta} = 0.901$	277.778	557.556	557.593	558.651
DIR	$\widehat{\theta} = 0.554$	186.547	375.094	375.131	376.189
DIW	$\widehat{\beta} = 1.049, \widehat{\theta} = 0.581$	172.935	349.869	349.982	352.060
Poi	$\widehat{\alpha} = 1.390$	246.210	494.420	494.457	495.515
DB	$\widehat{\alpha} = 0.278, \widehat{\beta} = 1.053$	171.139	346.278	346.391	348.469
DLogL	$\widehat{\alpha} = 0.780, \widehat{\beta} = 1.208$	171.717	347.430	347.550	349.620
DFx-I	$\widehat{\alpha} = 0.623$	182.288	366.575	366.612	367.671
DPa	$\widehat{\alpha} = 0.268$	171.192	344.384	344.421	345.479
DLo	$\widehat{\alpha} = 0.152, \widehat{\beta} = 1.830$	170.481	344.961	345.073	347.152
Geo	$\widehat{\theta} = 0.582$	178.767	359.533	359.570	360.629
GGeo	$\widehat{\beta} = 0.188, \widehat{\theta} = 0.800$	168.556	341.113	341.225	343.303
NeBi	$\widehat{\alpha} = 0.812, \widehat{\beta} = 0.322$	168.544	340.090	344.489	343.279

Table 21. The goodness–of–fit test for Dataset II (Part II).

		Expected frequencies							
X	ObFr	EDBuE	DLi-I	DLi-II	DLi-III	DR	DIR	DIW	Poi
0	65	64.590	40.286	46.026	46.008	10.890	60.888	63.910	27.398
1	14	16.235	29.834	26.768	26.765	26.618	33.990	20.699	38.084
2	10	9.065	18.357	15.568	15.570	29.448	8.123	8.053	26.468
3	6	5.729	10.336	9.054	9.058	22.296	3.004	4.234	12.264
4	4	3.852	5.523	5.266	5.269	12.629	1.420	2.599	4.262
5	2	2.691	2.851	3.062	3.066	5.539	0.779	1.754	1.185
6	2	1.931	1.437	1.781	1.783	1.914	0.473	1.261	0.274
7	2	1.412	0.711	1.036	1.037	0.526	0.308	0.949	0.054
8	1	1.048	0.347	0.602	0.604	0.116	0.212	0.739	0.009
9	1	0.786	0.167	0.350	0.351	0.020	0.152	0.592	0.001
10	1	0.596	0.079	0.204	0.204	0.003	0.112	0.485	0
11	2	2.065	0.072	0.283	0.285	0.001	0.539	4.725	0.001
Total	110	110	110	110	110	110	110	110	110
χ^2		0.637	34.635	19.091	19.096	306.515	40.456	6.445	89.277
df		3	4	3	2	4	2	3	3
P-value		0.888	< 0.001	0.0003	< 0.0001	< 0.001	< 0.001	0.092	< 0.001

Table 22. The goodness–of–fit test for Dataset II (Part III).

		Expected frequencies							
X	ObFr	DB	DLogL	DFx-I	DPa	DLo	Geo	GGeo	NeBi
0	65	64.743	63.192	45.256	65.842	61.615	45.980	62.738	56.520
1	14	19.177	20.101	29.094	18.267	21.023	26.760	19.665	15.885
2	10	8.484	8.644	16.508	8.164	9.687	15.575	9.439	9.173
3	6	4.632	4.656	8.893	4.513	5.275	9.064	5.436	6.203
4	4	2.863	2.864	4.703	2.820	3.197	5.275	3.463	4.502
5	2	1.920	1.921	2.489	1.909	2.088	3.070	2.349	3.400
6	2	1.365	1.368	1.335	1.368	1.441	1.787	1.663	2.635
7	2	1.013	1.019	0.731	1.022	1.038	1.039	1.213	2.079
8	1	0.777	0.786	0.409	0.789	0.773	0.605	0.904	1.663
9	1	0.613	0.623	0.234	0.626	0.592	0.352	0.685	1.344
10	1	0.494	0.504	0.137	0.506	0.463	0.205	0.525	1.095
11	2	3.919	4.322	0.211	4.174	2.808	0.288	1.920	5.501
Total	110	110	110	110	110	110	110	110	110
χ^2		2.587	4.033	31.702	3.430	3.238	19.109	2.444	4.287
df		2	3	4	4	3	4	3	4
P-value		0.274	0.258	< 0.001	0.489	0.356	< 0.001	0.485	0.369

Table 23. Descriptive statistics of Dataset II.

Model	Mean	Variance	Skewness	Kurtosis	IoD
Observed	1.391	6.112	2.293	8.174	4.394
Empirical	1.397	7.576	3.624	22.956	5.422

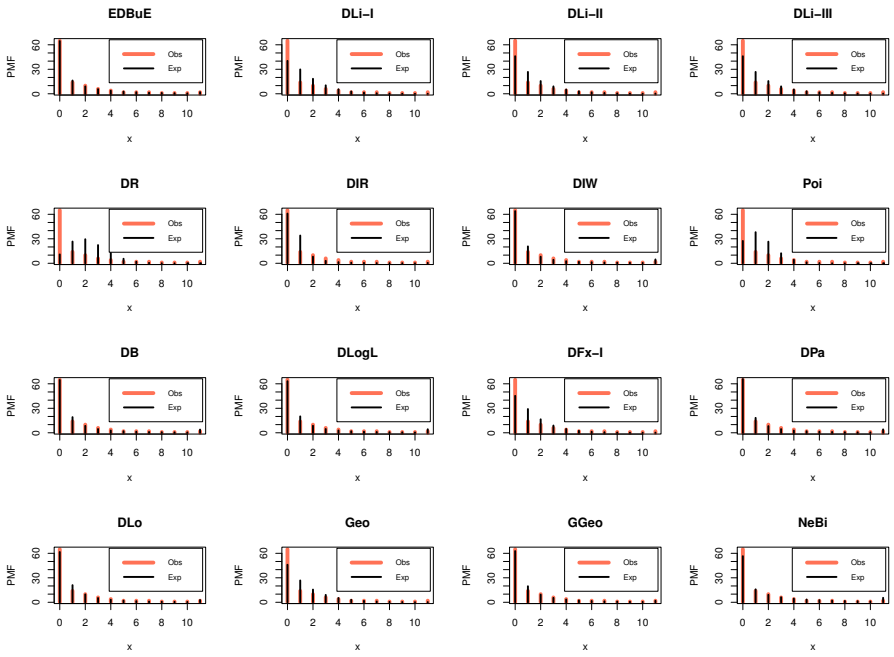

Figure 11. The observed and expected PMFs for Dataset II.

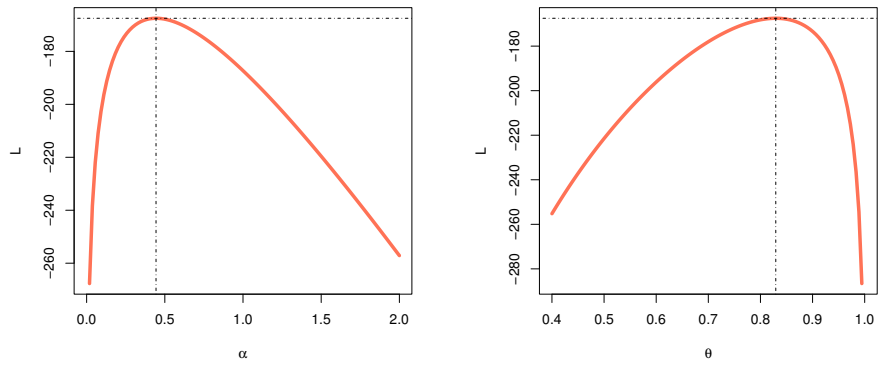

Figure 12. The log-likelihood profile of the model estimators based on Dataset II.

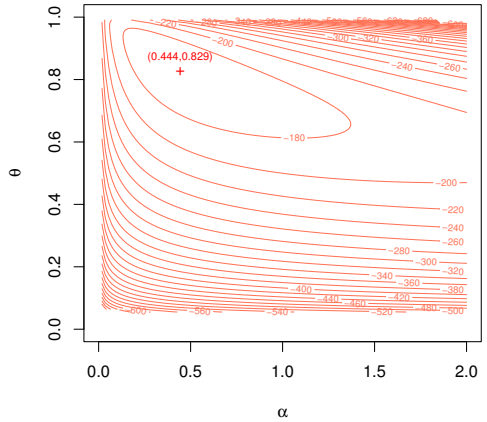

Figure 13. Contour diagrams of the model estimators based on Dataset II.

9.3. *Dataset III: Agricultural entomology / acarology*

This dataset records European red mite (*Panonychus ulmi*) counts on apple leaves, studied by the researchers in [2]. The discrete, non-negative count data exhibits overdispersion (variance exceeding mean) due to clustered pest distributions and potential zero-inflation from uninfested leaves, making it ideal for evaluating advanced discrete models such as the EDBuE distribution.

Figure 14 presents nonparametric diagnostics showing strong right-skewness, overdispersion, an extended upper tail, and deviation from normality, highlighting the need for flexible discrete modeling. Tables 24 and 25 demonstrate the EDBuE distribution's superior performance: It achieves the lowest information criteria (AIC = 449.749, CAIC = 449.831, HQIC = 452.195) and best goodness–of–fit (χ^2 = 2.896, p = 0.408), confirming optimal fit-parsimony balance and excellent agreement between observed and expected frequencies. Figure 15 visually confirms close alignment between observed and fitted PMFs, particularly in capturing high frequencies at low counts and the gradual tail decline. Figure 16 shows likelihood profiles with clear unimodal structures, verifying unique, well-defined MLEs and stable estimation without multiple local optima, thus establishing the EDBuE distribution as the most suitable model for this overdispersion, and right-skewed mite count data.

Figure 17 illustrates the contour diagrams of the parameter estimators for the EDBuE model applied to Dataset III. Table 26 presents the descriptive statistics for Dataset III. The observed and empirical data validate a right-skewed distribution characterized by overdispersion, wherein the variance surpasses the mean, hence necessitating the use of adaptable discrete models.

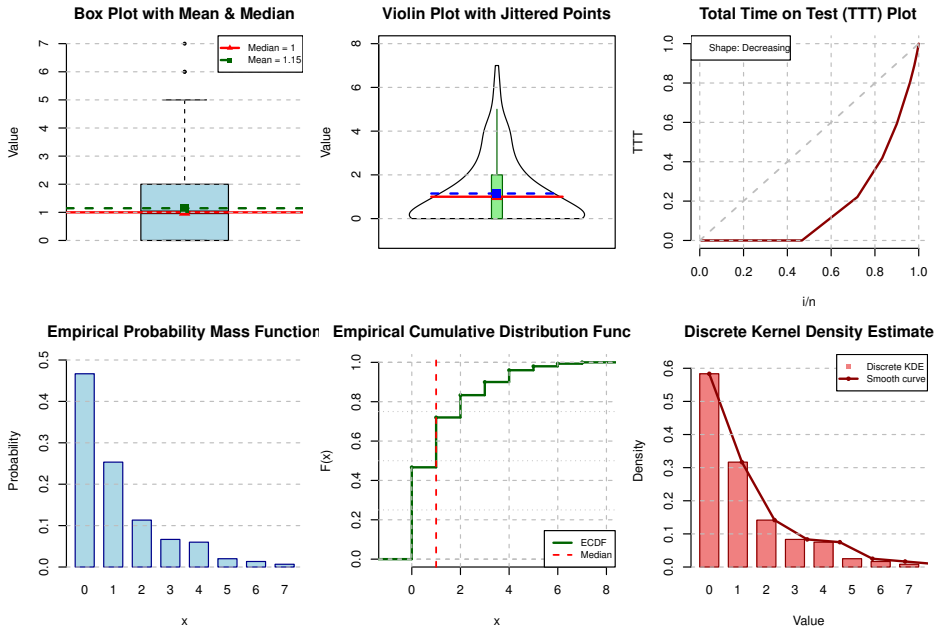

Figure 14. Nonparametric plots for Dataset III.

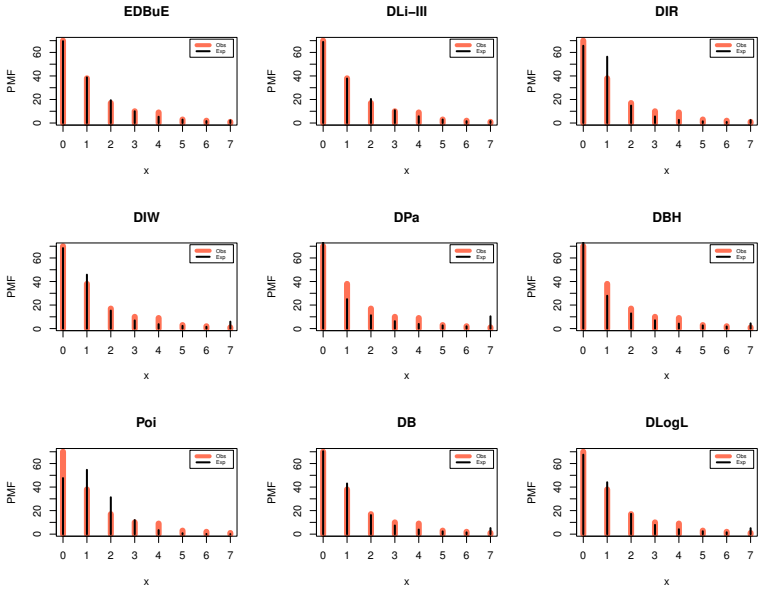

Figure 15. The observed and expected PMFs for Dataset III.

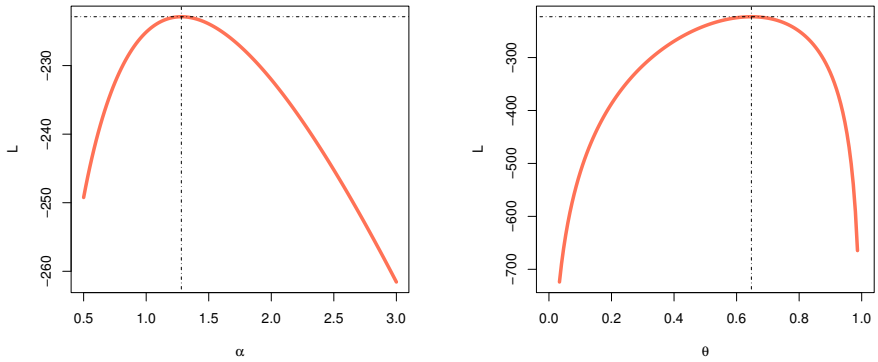

Figure 16. The log-likelihood profile of the model estimators based on Dataset III.

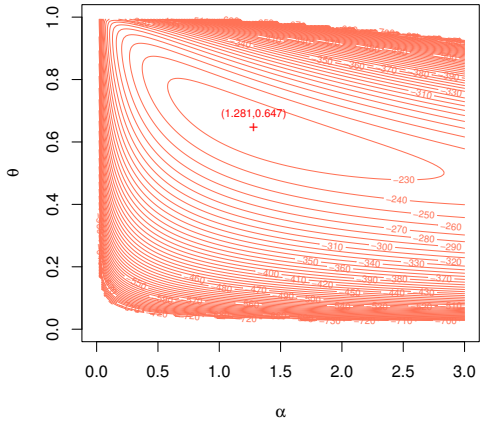

Figure 17. Contour diagrams of the model estimators based on Dataset III.

Table 24. The MLEs and goodness–of–fit tests for Dataset III.

Model	**MLEs**	$-L$	**AIC**	**CAIC**	**HQIC**
EDBuE	$\widehat{\alpha} = 1.281, \widehat{\theta} = 0.647$	222.275	449.749	449.831	452.195
DLi-III	$\widehat{\alpha} = 1.468, \widehat{\beta} = 0.228, \widehat{\lambda} = 0.479$	222.383	450.765	450.390	454.435
DIR	$\widehat{\theta} = 0.438$	233.142	468.284	468.311	469.507
DIW	$\widehat{\alpha} = 0.456, \widehat{\beta} = 1.527$	229.333	462.666	462.747	465.112
DPa	$\widehat{\alpha} = 0.278$	238.832	479.663	479.690	480.886
DBH	$\widehat{\alpha} = 0.814$	230.552	463.103	463.130	464.326
Poi	$\widehat{\alpha} = 1.147$	242.809	487.619	487.647	488.843
DB	$\widehat{\alpha} = 0.400, \widehat{\beta} = 1.882$	227.727	459.454	459.536	461.901
DLogL	$\widehat{\alpha} = 1.116, \widehat{\beta} = 1.829$	227.265	458.531	458.613	460.977

Table 25. The goodness–of–fit test for Dataset III.

		Expected frequencies								
X	ObFr	EDBuE	DLi-III	DIR	DIW	DPa	DBH	Poi	DB	DLogL
0	70	69.566	68.902	65.658	68.411	88.308	88.938	47.654	70.469	67.527
1	38	38.816	37.819	56.351	45.814	25.005	27.919	54.643	43.053	44.099
2	17	19.393	20.423	14.835	15.307	11.314	12.905	31.329	16.214	17.266
3	10	10.026	10.889	5.608	6.935	6.312	7.056	11.975	7.364	7.874
4	9	5.357	5.746	2.673	3.777	3.972	4.238	3.433	3.924	4.167
5	3	2.939	3.007	1.473	2.311	2.705	2.702	0.787	2.338	2.458
6	2	1.646	1.562	0.895	1.530	1.948	1.795	0.150	1.509	1.569
7	1	2.257	1.652	2.507	5.915	10.436	4.447	0.029	5.129	5.040
Total	150	150	150	150	150	150	150	150	150	150
χ^2		2.896	2.515	17.376	11.306	26.916	15.573	26.646	8.829	7.843
df		3	2	3	3	4	4	2	2	2
P-value		0.408	0.284	≤ 0.001	0.010	≤ 0.001	0.004	≤ 0.001	0.0121	≤ 0.001

Table 26. Descriptive statistics for Dataset III.

Model	Mean	Variance	Skewness	Kurtosis	IoD
Observed	1.147	2.274	1.545	1.315	1.983
Empirical	1.152	2.637	2.402	12.053	2.290

10. Concluding remarks

This work presented a novel discrete probability model aimed at addressing the varied data patterns commonly encountered in applied science. This distribution demonstrated substantial enhancements compared to current discrete lifespan models due to its adaptability and theoretical robustness. The theoretical framework was constructed by deriving the probability mass function, cumulative distribution function, and survival function. The asymptotic behavior of the distribution

was analyzed as the support variable neared zero and infinity. A study of the convexity of the probability mass function revealed the model's capacity to depict a range of geometries, from significantly skewed to nearly symmetric patterns. Following these essential characteristics, focus shifted to the model's reliability features. The functions for both the failure rate and the reversed failure rate were assessed. The investigation verified that the distribution accommodated a diverse array of hazard rate patterns, including declining, increasing, bathtub, J-shaped, and unimodal, contingent upon the parameter values. Moreover, the aging features of the distribution were categorized, pinpointing specific situations that aligned with classifications such as increasing failure rate, reducing failure rate, and new better than used. In addition to reliability engineering, the particular requirements of risk management were considered. Fundamental actuarial indicators, namely value-at-risk and tail value-at-risk, were calculated. Monte Carlo simulations corroborated these metrics, affirming their precision and reliability for practical applications such as determining insurance premiums and distributing resources. The distribution was further defined by deriving moment-based statistics, such as variance, index of dispersion, skewness, and kurtosis. To enable computational execution, the quantile function was formulated, and an algorithm for random variate generation was created via the inverse transform method. Entropy metrics, including Shannon and Rényi entropy, were computed to quantify the information content of the distribution. Maximum likelihood estimate methods were developed for practical application in both complete and type II censored samples. The requisite likelihood functions and scoring equations were established, employing the Newton–Raphson approach to determine parameter estimations. The methodologies were assessed via a comprehensive Monte Carlo simulation analysis comprising ten thousand replications. The findings indicated that the estimators functioned effectively, with little bias and a mean squared error that diminished with an increase in sample size. The research also validated that the estimating technique continued to be effective using censored data, notwithstanding the anticipated rise in variability. The model's efficacy was ultimately illustrated through the analysis of real-world datasets. The proposed distribution demonstrated a superior fit relative to competing models, as indicated by established model selection criteria. These applications underscored the distribution's adaptability and its utility for representing discrete lifetime and count data in practical contexts.

Author contributions

Mohamed S. Eliwa: Conceptualization, Formal analysis, Methodology, Software, Validation, Writing–review and editing; Hend S. Shahen: Data curation, Formal analysis, Investigation, Resources, Software, Validation; Mahmoud El-Morshedy: Data curation, Investigation, Methodology, Resources, Software, Writing–review and editing. All authors have read and agreed to the published version of the manuscript.

Use of Generative-AI tools declaration

The authors declare that they have not used Artificial Intelligence (AI) tools in the creation of this article.

Acknowledgments

The authors extend their appreciation to Prince Sattam bin Abdulaziz University for funding this research work through the project number (PSAU/2025/01/33334).

Conflict of interest

The authors declare no conflict of interest.

References

1. D. Roy, Discrete Rayleigh distribution, *IEEE Trans. Reliab.*, **53** (2004), 255–260. https://doi.org/10.1109/TR.2004.829161
2. S. Chakraborty, D. Chakravarty, Discrete gamma distributions: Properties and parameter estimations, *Commun. Stat.-Theory Meth.*, **41** (2012), 3301–3324. https://doi.org/10.1080/03610926.2011.563014
3. S. J. Almalki, S. Nadarajah, A new discrete modified Weibull distribution, *IEEE Trans. Reliab.*, **63** (2014), 68–80. https://doi.org/10.1109/TR.2014.2299691
4. V. Nekoukhou, H. Bidram, The exponentiated discrete Weibull distribution, *Sort-stat. Oper. Res. Trans.*, **39** (2015), 127–146.
5. E. Altun, M. El-Morshedy, M. S. Eliwa, A study on discrete Bilal distribution with properties and applications on integervalued autoregressive process, *REVSTAT-Stat. J.*, **20** (2022), 501–528.
6. E. M. Almetwally, S. Dey, S. Nadarajah, An overview of discrete distributions in modelling COVID-19 data sets, *Sankhya A*, **85** (2023), 1403–1430. https://doi.org/10.1007/s13171-022-00291-6
7. C. Chesneau, J. Gillariose, J. Joseph, A. Tyagi, New discrete trigonometric distributions: estimation with application to count data, *Int. J. Model. Simul.*, **45** (2024), 2072–2087. https://doi.org/10.1080/02286203.2024.2315328
8. M. S. Eliwa, M. El-Morshedy, A discrete extension of the exponential type II distribution: Statistical characterizations, reliability analysis, and Bayesian vs. non-Bayesian inferences for random right-censored and complete count data, *Jpn. J. Stat. Data Sci.*, **8** (2025), 279–317. https://doi.org/10.1007/s42081-024-00277-8
9. A. Pandey, R. P. Singh, A. Tyagi, An inferential study of discrete Burr-Hatke exponential distribution under complete and censored data, *Reliab.: Theory Appl.*, **17** (2022), 109–122. https://doi.org/10.24412/1932-2321-2022-471-109-122
10. S. Chakraborty, R. Gupta, Generating discrete analogues of continuous probability distributions: A survey of methods and constructions, *J. Stat. Distrib. Appl.*, **2** (2015), 6. https://doi.org/10.1186/s40488-015-0028-6

11. C. Kuş, A new lifetime distribution, *Comput. Stat. Data Anal.*, **51** (2007), 4497–4509. https://doi.org/10.1016/j.csda.2006.07.017

12. M. Ibrahim, H. Al-Mofleh, A. Z. Afify, The exponentiated negative binomial distribution, *Filomat*, **36** (2022), 4069–4087.

13. M. El-Morshedy, M. S. Eliwa, H. Nagy, A new two-parameter exponentiated discrete Lindley distribution: Properties, estimation and applications, *J. Appl. Stat.*, **47** (2020), 354–375. https://doi.org/10.1080/02664763.2019.1638893

14. J. P. Klein, M. L. Moeschberger, *Survival Analysis: Techniques for Censored and Truncated Data*, New York: Springer, 2003.

15. H. Krishna, N. Goel, Maximum likelihood and Bayes estimation in randomly censored geometric distribution, *J. Probab. Stat.*, 2017. https://doi.org/10.1155/2017/4860167

16. R. P. De Oliveira, M. V. de Oliveira Peres, E. Z. Martinez, J. A. Achcar, Use of a discrete Sushila distribution in the analysis of right-censored lifetime data, *Model Ass. Stat. Appl.*, **14** (2019), 255–268. https://doi.org/10.3233/MAS-190465

17. P. L. Ramos, D. C. Guzman, A. L. Mota, D. A. Saavedra, F. A. Rodrigues, F. Louzada, Sampling with censored data: A practical guide, *J. Stat. Comput. Simul.*, **94** (2024), 4072–4106. https://doi.org/10.1080/00949655.2024.2409379

18. R. Alotaibi, H. Rezk, E. M. Almetwally, Bayesian and non-Bayesian inference for discrete model based on censored samples with optimal test plan, *Rev. Int. Metodos Numer. Calc. Diseno Ing.*, **42** (2026), 20. https://doi.org/10.23967/j.rimni.2025.10.70966

19. S. Goliforushani, M. Asadi, On the discrete mean past lifetime, *Metrika*, **68** (2008), 209–217.

20. N. Balakrishnan, V. Leiva, A. Sanhueza, E. Cabrera, Mixture inverse Gaussian distributions and its transformations, moments and applications, *Statistics*, **43** (2009), 91–104. https://doi.org/10.1080/02331880701829948

21. S. Chan, P. R. Riley, K. L. Price, F. McElduff, P. J. Winyard, Corticosteroid-induced kidney dysmorphogenesis is associated with deregulated expression of known cystogenic molecules, as well as Indian hedgehog, *Amer. J. Physiol.-Renal Physiol.*, **298** (2009), 346–356. https://doi.org/10.1152/ajprenal.00574.2009

Appendix

Abbreviations

Abbreviation	Full Form
A-D	Anderson-Darling
AIC	Akaike Information Criterion
AL	Average Length
CAIC	Corrected Akaike Information Criterion
CDF	Cumulative Distribution Function
CI	Confidence Interval
CoEy	Collision Entropy
CP	Coverage Probability
DBuE	Discrete Burr-Hatke Exponential
df	Degree of Freedom
DFR	Decreasing Failure Rate
EDBuE	Exponentiated Discrete Burr-Hatke Exponential
FIM	Fisher Information Matrix
HQIC	Hannan-Quinn Information Criterion
HRF	Hazard Rate Function
IFR	Increasing Failure Rate
IoD	Index of Dispersion
K-S	Kolmogorov-Smirnov
MEy	Min-Entropy
MGF	Moment Generating Function
MLEs	Maximum Likelihood Estimators
MRE	Mean Relative Error
MSE	Mean Squared Error
ObFr	Observed Frequencies
OFIM	Observed Fisher Information Matrix
PMF	Probability Mass Function
REy	Rényi Entropy
RHRF	Reversed Hazard Rate Function
RMSE	Root Mean Squared Error
SF	Survival Function
SnEy	Shannon Entropy
TVaR	Tail Value at Risk
VaR	Value at Risk
XEy	Max-Entropy